

Simultaneous ram pressure and tidal stripping; how dwarf spheroidals lost their gas

Lucio Mayer ¹, Chiara Mastropietro¹, James Wadsley², Joachim Stadel ¹
 & Ben Moore ¹

¹*Institute of Theoretical Physics, University of Zürich, Winterthurerstrasse 190, 8057 Zurich, Switzerland*

²*Department of Physics & Astronomy, McMaster University, 1280 Main St. West, Hamilton ON L8S 4M1 Canada*

12 September 2018

ABSTRACT

We perform high-resolution N-Body+SPH simulations of gas-rich dwarf galaxy satellites orbiting within a Milky Way-sized halo and study for the first time the combined effects of tides and ram pressure. The structure of the galaxy models and the orbital configurations are chosen in accordance to those expected in a Λ CDM Universe. While tidal stirring of disk-like dwarfs produces objects whose stellar structure and kinematics resembles that of dwarf spheroidals after a few orbits, ram pressure stripping is needed to entirely remove their gas component. Gravitational tides can aid ram pressure stripping by diminishing the overall potential of the dwarf, but tides also induce bar formation which funnels gas inwards making subsequent stripping more difficult. This inflow is particularly effective when the gas can cool radiatively. Assuming a low density of the hot Galactic corona consistent with observational constraints, dwarfs with $V_{peak} < 30$ km/s can be completely stripped of their gas content on orbits with pericenters of 50 kpc or less. Instead, dwarfs with more massive dark haloes and $V_{peak} > 30$ km/s lose most or all of their gas content only if a heating source keeps the gas extended, partially counteracting the bar-driven inflow. We show that the ionizing radiation from the cosmic UV background at $z > 2$ can provide the required heating. In these objects most of the gas is removed or becomes ionized at the first pericenter passage, explaining the early truncation of the star formation observed in Draco and Ursa Minor. Galaxies on orbits with larger pericenters and/or falling into the Milky Way halo at lower redshift can retain significant amounts of the centrally concentrated gas. These dwarfs would continue to form stars over a longer period of time, especially close to pericenter passages, as observed in Fornax and other dSphs of the Local Group. The stripped gas breaks up into individual clouds pressure confined by the outer gaseous medium that have masses, sizes and densities comparable to the HI clouds recently discovered around M31.

Key words: methods: N-body simulations – galaxies:dwarfs – galaxies: interactions – galaxies:Local Group – hydrodynamics

1 INTRODUCTION

The origin of dwarf spheroidal galaxies (dSphs) is a long standing subject of debate. These galaxies are gas poor or completely devoid of gas and are the faintest galaxies known. Objects matching the definition of dSphs are found both in galaxy clusters and in groups, but it is certainly the Local Group the place where dSphs have been better studied thanks to their proximity.

Two main formation paths have been proposed to explain their origin, nature of nurture. In one scenario these faint galaxies could be the result of cosmic reionization and stel-

lar feedback quenching gas accretion and star formation in low mass haloes (Dekel & Silk 1986; Thoul & Weinberg 1996; Bullock, Kravtsov & Weinberg 2000; Ferrara & Tolstoy 2000 ; Benson et al. 2002a, 2002b; Somerville 2002; Susa & Umemura 2004). However, there is no obvious signature of reionization in the star formation history of these galaxies (Grebel & Gallagher 2004), which in many cases continued to form stars over more than 10 Gyr, and for some dSphs the most recent inferred halo masses are likely too large ($10^8 - 10^9 M_\odot$, see Kleyna et al. 2002; Wilkinson et al. 2004; Kazantzidis et al. 2004) for supernovae winds to

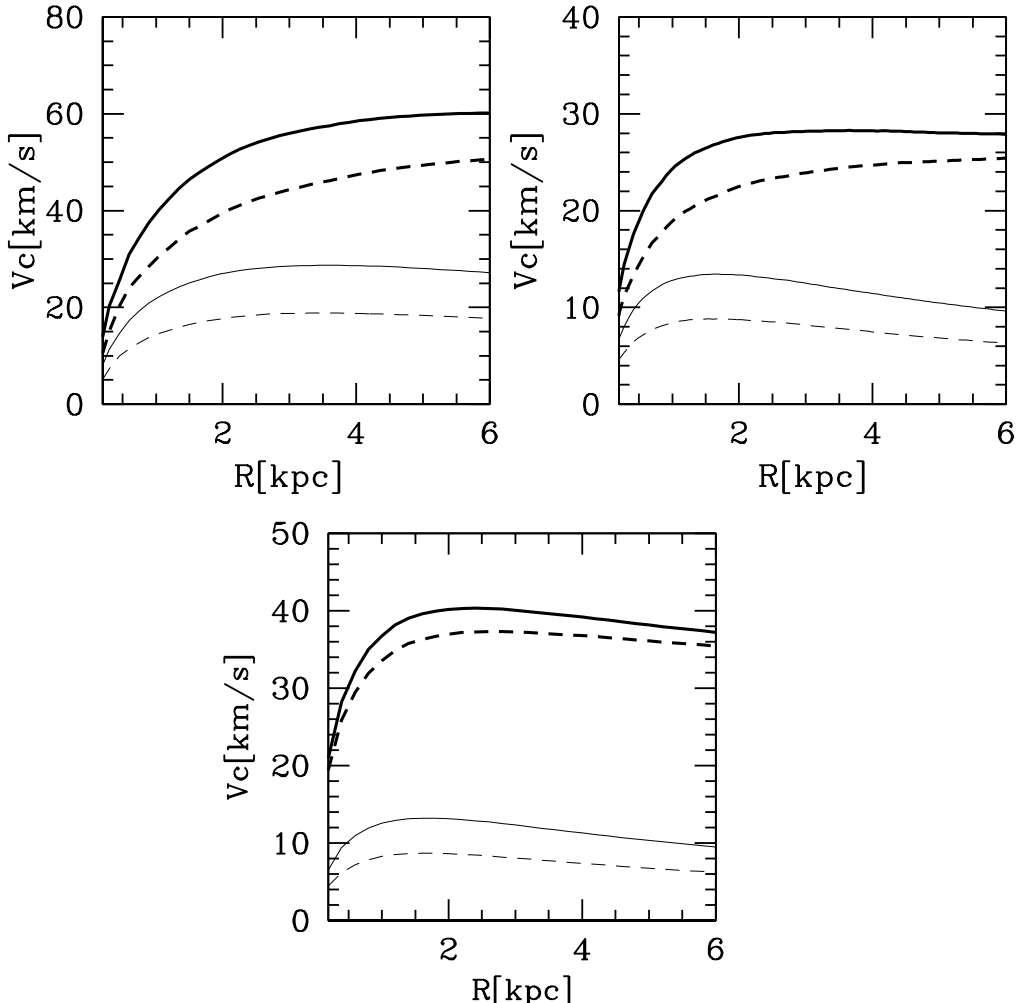


Figure 1. Initial rotation curves of the dwarf galaxy models. The lines show, respectively, the total rotation curve (thick solid), the contribution of dark matter (thick dashed), that of stars (thin solid) and that of gas (thin dashed). From top left to bottom, models V60c4, V30c4 and V40c20 are shown.

remove most of the baryons (Mori, Ferrara & Madau 2002; Mayer & Moore 2004; Read & Gilmore 2004).

In addition, these models do not naturally explain why dSphs share some structural similarities with equally faint but gas-rich, much younger disk-like galaxies, dwarf irregulars (dIrrs), notably their exponential light distribution. Furthermore they do not give rise to the morphology-density relation observed in groups and clusters, namely the fact that dSphs tend to be concentrated towards the central galaxies while dIrrs are found at much larger distances, nor they explain the dichotomy between dominance of rotation for the stars of most dIrrs and dominance of pressure support for those of dSphs. Various environmental effects have been scrutinized to explain similarities and differences between the two types of galaxies postulating that dSphs are somehow transformed dIrrs. Ram pressure stripping of gas from dwarf irregular-like progenitors caused by a hot diffuse gaseous corona surrounding the Milky Way has been proposed as a way to explain the low gas contents of dSphs together with the similar stellar light distributions of the

two types of dwarfs (Einasto et al. 1974; Faber & Lin 1983; Grebel, Gallagher & Harbeck 2003), and has also been considered as the origin of HI clouds possibly associated with some dSphs and transitional dIrrs/dSphs like Phoenix (Blitz & Robishaw 2000; Gallart et al. 2001). Van der Bergh (1996) has argued that the correlation between galactocentric distance and gas content in dSphs is a signature of ram pressure stripping. Tidal stripping of dwarf irregulars has also been considered as an alternative way of removing gas from the dwarfs (e.g. Ferguson & Binggeli 1994).

Recently, high resolution N-Body/SPH simulations were used to show that tides do not only remove gas and stars but can also reshape the stellar components of a dwarf disk galaxy resembling a dwarf irregular (Mayer et al. 2001a,b). This “tidal stirring” can turn a rotationally supported disk into a pressure supported spheroidal stellar system by means of bar formation and a subsequent buckling instability. The mechanism is particularly effective for satellites of massive galaxies that are strongly tidally shocked owing to the plunging orbits expected in CDM models and

works for systems having a variety of dark halo profiles, including cuspy profiles (Mayer et al. 2002). The transformation is not necessarily associated with intense tidal mass loss; indeed, objects with very high-mass-to light ratios, thus embedded in dense, massive dark halos, can still be reshaped from the instabilities induced by tidal shocks albeit losing minimal mass (Mayer et al. 2001b).

A problem of this model, however, is that tides cannot remove completely the gas from the disk progenitors of dSphs; the low gas fractions of dSphs can be explained by only invoking rapid consumption from star formation of the remaining gas in a series of tidally triggered bursts associated with bar-driven gas inflows (Mayer et al. 2001b). However, although intermittent star formation is observed in some dSphs (Gallart et al. 1999; Hernandez, Gilmore & Valls-Gabaud 2000), the star formation rates needed to completely consume the gas are well in excess of those implied by reconstructions of the star formation histories of dSphs using detailed color-magnitude diagrams (Mayer et al. 2001b). Moreover, Draco and a few other dSphs do not show extended star formation histories, instead seem to have ceased star formation about 10 Gyr ago (Grebel et al. 2004).

It is likely that both gravitational tides and hydrodynamical processes play a role (Gavazzi et al. 2001). For example, ram pressure could act simultaneously with tides and increase the efficiency of gas removal (Mayer & Wadsley 2003). Recent 2D and 3D grid-based hydrodynamical simulations of ram pressure stripping of disk-like dwarfs in poor groups show that ram pressure alone can remove most of the gas in dwarf galaxies with halo circular velocities lower than 30 km/s (Marcolini, Brighenti & D'Ercole 2003). However, these and other simulations (Mori & Burkert 2000) do not use models of dwarf galaxies directly based on the Λ CDM model and do not include the effect of tides. The effectiveness of both ram pressure and tidal stirring will also depend on the orbital history of the dwarfs, and this is where the cosmological framework comes into play. For example dwarfs that fell into the primary halo at very high redshift likely had orbits with smaller pericenters relative to those falling later on (Mayer et al. 2001b), thus suffering stronger tidal shocks, and possibly also stronger ram pressure in a denser gaseous corona, while being exposed to the effect of the cosmic UV background (Bullock, Kravtsov & Weinberg 2000; Somerville 2002; Barkana & Loeb 1999; Shaviv & Dekel 2003). Indeed cosmological simulations of galaxy formation incorporate all such mechanisms but their resolution is still too coarse to allow a study of their effects at the scale of the tiny dwarf spheroidals (Governato et al. 2004).

In this paper we will study for the first time the combined effects of ram pressure and tidal stirring using high resolution three dimensional N-Body+SPH simulations of dwarf galaxies orbiting within the Milky Way dark halo and gaseous corona. We will use galaxy models and orbits consistent with the predictions of Λ CDM simulations. The simulations include also radiative cooling as well as heating and ionization from the cosmic UV background radiation. The main goal of the present work will be to establish whether these two mechanisms can explain the present-day low gas content of dSphs if these galaxies are the descendants of gas-rich dwarfs with structure similar to today's dIrrs.

2 INITIAL CONDITIONS

2.1 Galaxy models

Models comprise an exponential disk of gas and stars embedded in a live NFW halo for the dwarf, and a live NFW halo plus hot gas distribution with the same density profile for the primary galaxy. Halo virial parameters (mass, radius, circular velocity) are consistent with the LCDM model. Although we believe that the Milky Way halo has a virial velocity $V_{vir} = 140 - 160$ km/s (Klypin, Zhao & Somerville 2002) we use a slightly larger value, $V_{vir} = 180$ km/s, in order to have $V_{peak} = 230$ km/s at about 10 kpc from the center without including a disk component. We choose a concentration $c = 10$ for the MW halo, this being typical for LCDM halos at a scale of $\sim 10^{12} M_\odot$ (Bullock et al. 2001). With our choice of parameters the shape of the rotation curve is quite flat out to 100 kpc and the resulting halo mass within 100 kpc is $\sim 8 \times 10^{11} M_\odot$, consistent with the orbital dynamics of the Magellanic Clouds and distant dSphs (Lin, Jones & Klemola 1995; Dehnen & Binney 1998). Overall our halo model resembles model A3 in Klypin, Zhao & Somerville (2002), which matches simultaneously most of the known observational constraints within the framework of the LCDM model. The hot gas is in hydrostatic equilibrium within the halo potential and its temperature is $\sim 10^6$ K at 50 kpc, consistent with OVI, OVII and X-ray absorption measurements in the Galactic halo (Sembach et al. 2003). Assuming an isotropic model, the halo temperature at a given radius r is determined by the cumulative mass distribution $M(r)$ of the dark, stellar and gaseous components of the MW beyond r and by the density profile $\rho_h(r)$ of the hot gas:

$$T(r) = \frac{m_p}{k_B} \frac{1}{\rho_h(r)} \int_r^\infty \rho_h(r) \frac{GM(r)}{r^2} dr, \quad (1)$$

where m_p is the proton mass, G and k_B are the gravitational and Boltzmann constants. Its density at 50 kpc from the center is 8×10^{-5} atoms/cm³ (see also Mastropietro et al. 2004). At a distance of ~ 100 kpc or more, where the dwarf galaxies that we have simulated spend most of the time while orbiting within the primary halo (see below), the hot halo density is $< 10^{-5}$ atoms/cm³. Such a hot diffuse halo is also a natural expectation of the current LCDM paradigm of structure formation (White & Frenk 1991; Governato et al. 2004; Sommer-Larsen, Portinari & Goetz 2003; Maller & Bullock 2004).

The multi-component dwarf galaxy models are built using the technique developed by Hernquist (1993) and later refined by Springel & White (1999) (for further details on the modeling see also Mayer et al. 2002). They comprise an exponential disk of gas and stars embedded in an NFW halo. We used three dwarf models with $V_{peak} = 28, 42$ or 62 km/s km/s and concentration $c = 4$ (the first two models) and $c = 20$ (the third model). The choice of halo concentration can be quite flexible since cosmological simulations show a large scatter of such property at small mass scales, mostly due to a large spread in halo formation times (Bullock et al. 2001). The rotation curves of the models are reported in Figure 1; while the rotation curves of models V60c4 and V30c4 are slowly rising in agreement with those of today's dwarf irregulars, that of model V40c20 rises quite steeply owing to the much higher halo concentration. A steep rota-

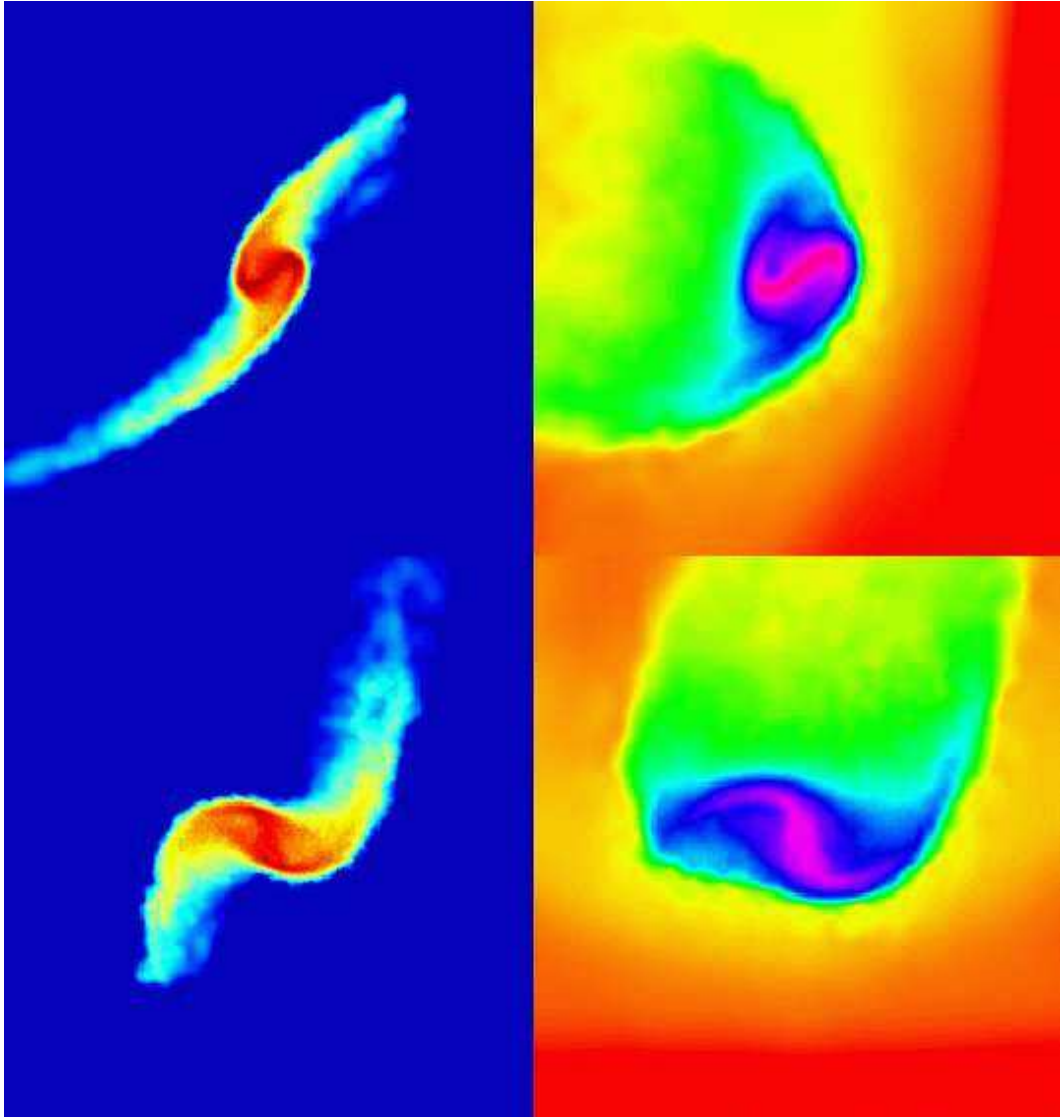


Figure 2. Color coded logarithmic density maps for run Rc4aADHR. Projections along (top) and perpendicular to the orbital plane (bottom) are shown for the stars (left) and for the gas component (right). Snapshots are taken at $T = 1.7$ Gyr, while crossing pericenter for the first time. Boxes are 100 kpc on a side for the stars and 30 kpc on a side for the gas (a smaller box is used for the gas to show its structure in greater detail). The two color maps are such that colors go, respectively, from blue to red through yellow (stars) and from red to magenta through yellow and green (gas) going from lower to higher densities.

tion curve is a more appropriate choice for the progenitors of Draco or Ursa Minor that have very high central dark matter densities (see Mayer et al. 2001b; Hogan & Dalcanton 2000).

Lokas (2002) and Kazantzidis et al. (2004) have shown that dSphs kinematics suggests they are embedded in halos with $V_{peak} \sim 20 - 35$ km/s. We used even larger values of V_{peak} in our initial conditions since these can later decrease as a result of tidal mass loss, by roughly a factor of 2 according to the recent cosmological simulations by Kravtsov, Gnedin & Klypin (2004).

The galaxy models have disks of mass $\approx 4\%$ of the total mass, lower than the universal baryon fraction but quite typical for present-day LSB or dIrr galaxies (Jimenez et al. 2003). Following, Mo, Mao & White (1998), the exponential scale length R_h of the disk is determined by the spin pa-

rameter and concentration c of the halo; we use $\lambda = 0.043$ for models Rc4a and Rc4b, and $\lambda = 0.08$ for model Rc20a,b (the mean spin of cosmological halos is $\lambda \sim 0.05$, see e.g. Gardner 2001, and 20% of halos have spins as high as 0.1 due to the log-normal shape of the probability distribution of halo spins). The disk sizes in models V28c4 and V40c20 are the same (the higher spin parameter compensates for the higher halo concentration) and, since also the disk mass is the same by choice, we can isolate the role of halo concentration (or, equivalently, V_{peak}) by comparing the two models. Note that all the models have a central surface brightness of 23 mag arcsec $^{-2}$ in the B band for a stellar-mass-to light ratio of 2, typical of dIrrs and dwarf spirals (see de Blok & McGaugh 1997). Galaxies with these low disk mass fractions are stable to bar formation in isolation irrespective on halo concentration (Mayer & Wadsley 2004). However they

Table 1. Parameters of the full interaction (FI) simulations. Column 1: Name of model Column 2: Peak circular velocity of the satellite (km/s) Column 3: Satellite halo concentration Column 4: Disk scale length (kpc) Column 5: Apocenter distance (kpc) Column 6: Pericenter distance (kpc) Column 7: Thermal physics (AD=adiabatic, RC=radiative cooling, RCUV=radiative cooling + cosmic UV background). All runs include tides and ram pressure except those referred to as TD which do not include ram pressure. Column 8: name of run (HR stands for high resolution, see text). Column 9: initial gas mass (in units of $10^6 M_\odot$) Column 10: final gas mass (in units of $10^6 M_\odot$)

Model	V_{peak}	c	R_h	r_{apo}	r_{peri}	physics	Run	M_{gas_i}	M_{gas_f}
V60c4	62	4	2.2	250	50	AD	Rc4aAD	450	55
V60c4	62	4	2.2	250	50	AD	Rc4aADHR	450	60
V60c4	62	4	2.2	250	50	RC	Rc4aRCHR	450	380
V60c4	62	4	2.2	250	50	RCUV	Rc4aRCUV	450	290
V28c4	25	4	1.1	250	50	TD(AD)	Rc4bTD	45	20
V28c4	25	4	1.1	250	50	AD	Rc4bAD	45	0
V28c4	25	4	1.1	250	50	RC	Rc4bRC	45	9.5
V28c4	25	4	1.1	150	30	RC	Rc4cRC	45	0
V40c20	42	20	0.5	150	30	TD(AD)	Rc20TD	46.5	22.2
V40c20	42	20	0.5	150	30	AD	Rc20AD	46.5	0
V40c20	42	20	0.5	150	30	RC	Rc20RC	46.5	3.55
V40c20	42	20	0.5	150	30	RCUV	Rc20RCUV	46.5	0.65
V40c20	42	20	0.5	250	50	AD	Rc20bAD	46.5	0
V40c20	42	20	0.5	250	50	RC	Rc20bRC	46.5	10

can become bar unstable when tidally perturbed by a much more massive halo.

We use 3×10^5 particles for the dark halos of the dwarfs and 3×10^4 particles for both the stellar and the gaseous disk of the dwarf. The Milky Way halo is modeled with 10^6 dark matter particles, while 5×10^5 particles are used for the superimposed gaseous halo (the mass of hot halo particles is $8 \times 10^4 M_\odot$). Each simulation has a total of $\sim 1.8 \times 10^6$ particles, which makes them quite computationally demanding. Two runs employing model V60c4 were repeated with increased resolution in the disk of the dwarf, (2×10^5 particles for both its stellar and its gaseous component, see Table 1). The choice of putting a large fraction of the total number of particles in the primary halo is motivated by the desire of minimizing spurious two-body heating between halo particles and those of the disks of the dwarfs (Moore, Katz & Lake 1996; Mayer 2004). We use a fairly large gravitational softening for the gas and dark matter particles in the primary system, $\varepsilon = 2$ kpc to minimize discreteness noise in the potential. For the dwarf models instead, the softening is $\varepsilon = 0.3R_h$ for halo particles and $\varepsilon = 0.1R_h$ for star and gas particles, where R_h is the disk scale length (see Table 1).

2.2 Simulations

The dwarf galaxy satellites are placed on bound eccentric orbits in the primary halo. In Mayer et al. (2001b) we explored a wide range of orbital eccentricities and initial disk inclinations. Tidally induced transformation was found to be essentially independent on disk inclination (with only purely retrograde encounters versus purely prograde encounters showing significant differences). We also found that the orbital time, and not the orbital eccentricity, is the most sensitive orbital parameter for causing the transformation since it determines both the strength and number of tidal shocks. Here we choose orbits with an apocenter to pericenter ratio of 5, corresponding to the mean value for satellites in cosmological simulations (Ghigna et al. 1998, Gill et al. 2004), and we consider apocenters of 250 or 150 kpc (the

pericenter being 50 or 30 kpc) corresponding to orbital times of, respectively, 3.2 and 1.3 Gyr. The dwarf galaxies start at apocenter and are evolved for 3 to 5 orbits with their disks initially inclined 60 degrees with respect to their orbital plane. Different mean orbital distances radii could be associated to satellites infalling into the Milky Way halo at different cosmic epochs (Mayer et al. 2001b; Kravtsov et al. 2004; Gill et al. 2004), say at $z > 1$ or $z < 1$, for, respectively, the smaller and larger orbital time.

The simulations were performed with the parallel Tree+SPH code GASOLINE (Wadsley, Stadel & Quinn 2004). The internal energy of the gas is integrated using the asymmetric formulation, that gives results very close to the entropy conserving formulation (Springel & Hernquist 2003) but conserves energy better. In simulations without radiative cooling the gas can heat or cool only by adiabatic compression or expansion. Dissipation in shocks is modeled using the quadratic term of the standard Monaghan artificial viscosity. The Balsara correction term is used to reduce unwanted shear viscosity (Balsara 1995). A detailed description of the SPH code is given in Wadsley et al. 2004.

We perform both adiabatic runs and runs with radiative cooling. We use a standard cooling function for a primordial mixture of hydrogen and helium (the metallicity in dSphs is indeed much lower than solar, with $-1 < \text{Fe/H}_i < -2$, see Gallagher, Grebel & Harbeck 2003). Cooling shuts off below 10^4 K. The initial temperature of the gaseous disks is 8000 K for the most massive model ($V_{max} = 62$ km/s) and slightly lower for the other lighter models. The purpose of running adiabatic simulations is two-fold; first, it helps in understanding the interplay between thermodynamical and mechanical effects of ram pressure as we shall see in the following section, and second heating by external radiation fields or stellar feedback, especially in low mass objects as those considered in this paper, might overtake radiative cooling and create a hot phase that would essentially behave as an adiabatic gas (Thacker & Couchman 2000; Marcolini et al. 2003; Springel & Hernquist 2003). Therefore radiative cooling and adiabatic runs can be regarded as two extreme

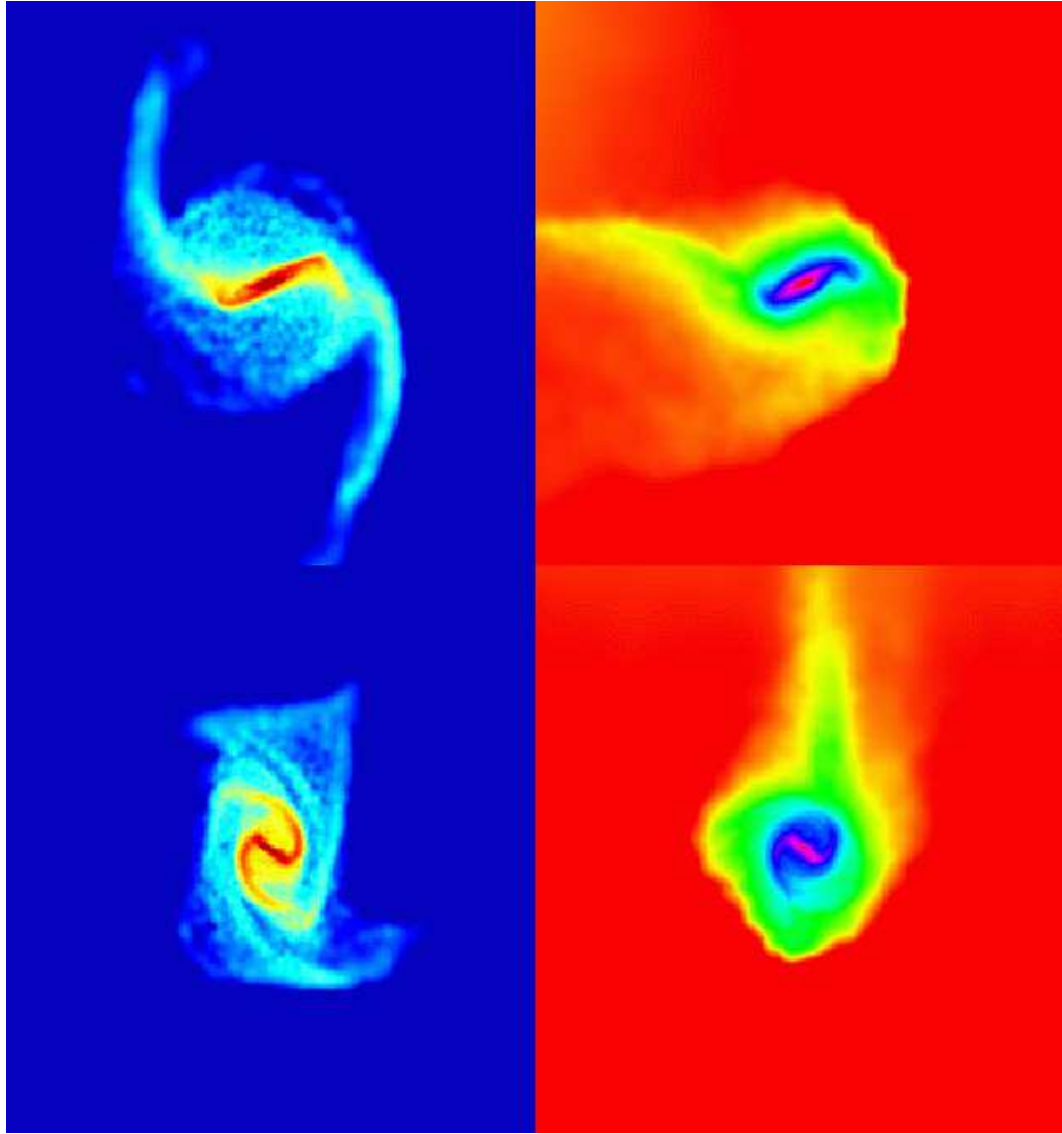


Figure 3. Color coded logarithmic density maps for run Rc4aADHR. Projections along (top) and perpendicular to the orbital plane (bottom) are shown for the stars (left) and for the gas component (right). Snapshots are taken at $T = 3$ Gyr, after first pericenter passage. Boxes are 50 kpc on a side.

Table 2. Parameters of the wind tunnel (WT) simulations. Column 1: Model Galaxy (see Table 1). Column 2: Gas physics (AD=adiabatic, RC=radiative cooling). Column 3: Angle between z-axis of the disk and direction of the flow. Column 4: Mass remaining in the disk at after 5×10^8 years (in units of $10^7 M_\odot$). Column 5: Stripping radius in kpc. Column 6: Stripping radius (in kpc) predicted using analytical prediction (see text). Column 7: name of run (LR stands for “low resolution”, see text).

Model	gas physics	i	M_{fin}	R_{strip1}	R_{strip2}	RUN
V28c4	AD	0	0	0	0	T1c4a
V28c4	AD	90	0	0	0	T2c4a
V28c4	RC	0	0	0	0	T3c4a
V28c4	RC	45	0	0	0	T4c4a
V28c4	RC	90	6	0	0	T5c4a
V60c4	AD	0	57	4.25	5.8	T1c4b
V60c4	AD	30	66	4.25	5.8	T2c4b
V60c4	AD	60	64	4.25	5.8	T3c4b
V40c20	AD	0	4.38	1.58	1.6	T1c20
V40c20	AD	0	3.6	1.5	1.6	T1c20LR
V40c20	RC	0	6.2	1.75	1.6	T2c20
V40c20	RC	90	7.85	2	1.6	T3c20

cases crudely bracketing the conditions of the real interstellar medium in which a hot and a cold phase will coexist at all times. Finally, in a few runs with cooling we also include a uniform external radiation field which models the cosmic UV background arising at high redshift. This is implemented using the Haardt & Madau (1996) model which includes photoionizing and photoheating rates produced by QSOs and galaxies starting at $z = 7$. We implicitly assume that the dwarf enters the Milky Way halo at $z = 7$. The ionizing flux remains quite high until $z = 2$, therefore the dwarf is exposed to the radiation for a duration of ~ 5 Gyr.

We complement our “full interaction” runs (hereafter FI runs), so called because they include both tides and ram pressure, with wind tunnel simulations aimed at studying the effect of ram pressure alone. The volume of the simulations is a tube with rectangular section, having a base equal to the diameter of the dwarf model (out to its virial radius) and height $h = vt$, where v is the typical velocity of the satellite at pericenter in the FI runs (290 km s^{-1}) and t is set ~ 0.5 Gyrs ($\gtrsim t_{enc} = R_{peri}/V_{peri}$, where t_{enc} is the time the dwarf spends near pericenter of the orbits in the FI runs). We represent the hot gas as a flux of particles moving with a velocity v along the longest axis of the tube, this being parallel or at an angle with the angular momentum of the disk depending on the run. The hot particles have an initial random distribution, a temperature $T = 10^6 \text{ K}$ and a number density $n_h = 8 \times 10^{-5} \text{ cm}^{-3}$. We use periodic boundary conditions in order to restore the flow of hot gas that leaves the tube. We will indicate these as WT runs (where WT stands for wind tunnel). These experiments allow to resolve the background gas flow with very high resolution, thus limiting numerical artifacts like the spurious stripping induced by transfer of momentum in two-body collisions between the hot halo particles and the gas particles in the disk of the dwarf (Abadi, Moore & Bower 1999). The mass of the gas particles is equal to that used for the dwarfs in the FI runs, i.e. $8 \times 10^4 M_\odot$, for the runs employing our largest dwarf model, V60c4, while it is 8 times lower for the runs employing the other two models, V28c4 and V40c20, since these have correspondingly lighter disks. The (adiabatic) runs with models V28c4 and V40c20 where repeated with a lower resolution of the background flow, equal to that of the FI runs. The total number of particles used in the hires WT runs thus varies from 10^6 in runs with models V28c4 and V40c20 to 2×10^5 in runs with model V60c4.

3 RESULTS

Table 1 and 2 report the results of the FI and WT runs. Dwarf galaxies undergo severe stripping owing to the combined action of tides and ram pressure. The overall mass loss varies depending on the dwarf galaxy model, in particular the depth of its potential well, on its orbit and on the gas physics (the balance between cooling and heating). Dwarfs can retain 20 – 50% of their initial gas content or be completely stripped. Ram pressure stripping occurs very rapidly as the galaxy approaches pericenter for the first time. A bow shock is visible (Figure 2) and reflects the fact that the dwarfs near pericenter are moving at mildly supersonic velocities in the hot halo owing to their eccentric orbits (the Mach number is ~ 1.5).

The tidal shock at first pericenter passage deforms the disk to an extent that depends on how deep is the potential well of the galaxy. Symmetric stellar tidal tails develop but the gas generally trails the galaxy since ram pressure sweeping dominates (compare gas and stars in Figure 3). The dark halo loses most of its mass in all cases and the overall depth of the potential well is reduced which increases the efficiency of gas removal. The stars develop a bar instability due to the strong tidal perturbation (Figure 3) which drives a radial gas inflow (Mayer et al. 2001b). This inflow counteracts the reduction of the mean restoring force by moving some gas deeper towards the center of the dwarf where it is harder to strip (note the central density concentration in Figure 4-6). As a result on subsequent orbits ram pressure stripping continues but with much lower intensity.

In what follows we will describe the results quantitatively by analyzing the gas mass loss in FI and WT runs as well as the fate of the stripped gas.

3.1 Gas mass loss

3.1.1 Wind tunnel (WT) runs

Figure 7-10 show the evolution of the gas component of the dwarfs. In the absence of an external perturbation the stellar disks are stable to bar formation. Removal of gas begins immediately; a bow shock develops and some gas in the disk rises above the disk plane slightly more than 10^7 years. This is evident in the early truncation of the gas surface density profiles (see Figure 12). The stripped gas is diffuse in adiabatic runs whereas it breaks into clumps pressure confined by the external medium in the cooling runs (see Figure 8). The evolution of the temperature of the gas is shown in Figure 11. As the hot halo pushes the gas out of the disk it also rises its temperature to $\sim 10^5 \text{ K}$ as a result of compression. If radiative cooling is included the gas quickly cools down to 10^4 K ; cooling occurs on a timescale shorter than 10^7 years since the gas is heated to temperatures at which the cooling rate is maximum. Occasionally gas particles that did not gain enough momentum to leave the disk fall back towards the midplane as they cool down (compare for example Figures 7 and 8 for run T2c20 - the disk appears more intact at a later time). The distribution of the gas becomes slightly more concentrated towards the midplane of the disk (see the evolution of the surface density profiles in Figure 12), and subsequent stripping is harder. In adiabatic runs, instead, the heated gas remains hot and expands; the gas disk thickens and it is stripped more easily than in the cooling runs (see Figure 8) as its own pressure support makes it less bound to the disk potential. No stripped gas falls back to the disk.

We consider as “stripped” all the gas that is removed from the stellar disk. Table 2 also includes the stripping radii found in the simulations, defined as the minimum distance from the center of the dwarf at which gas particles are stripped. Some of the WT runs were performed twice, using a resolution of the background flow equal or higher than that of the FI runs employing the same model (see section 2.2); we found differences within 20% for the gas mass loss and even less for the stripping radii. Table 2 reports the gas mass in the disk measured after 0.2 Gyr. The difference in the amount of stripped mass between runs with and with-

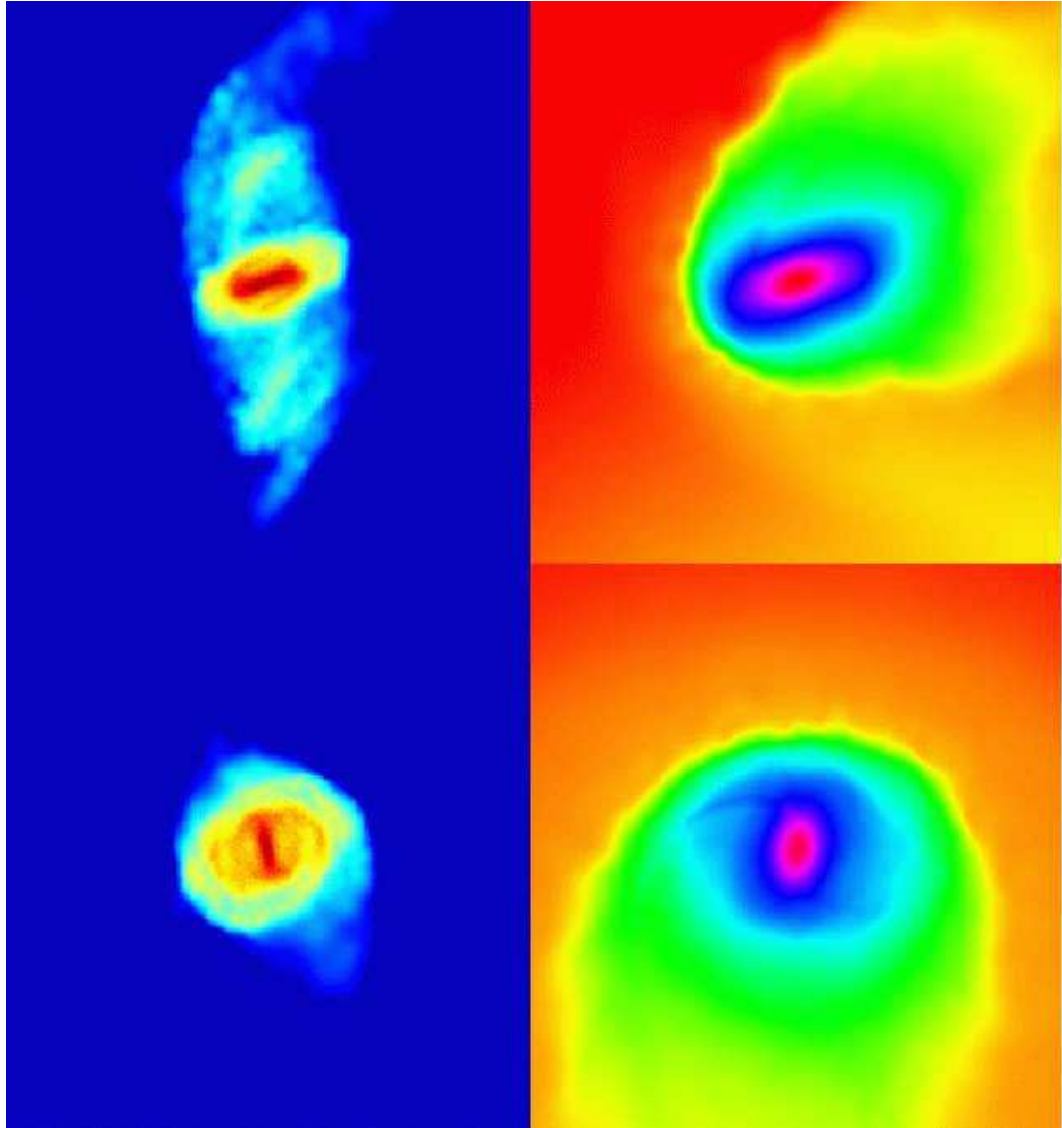


Figure 4. Color coded logarithmic density maps for run Rc4aADHR. Projections along (top) and perpendicular to the orbital plane (bottom) are shown for the stars (left) and for the gas component (right). Snapshots are taken at $T = 6$ Gyr, after the second pericenter passage. Boxes are 50 kpc on a side for the stars and 25 kpc on a side for the gas.

out cooling is visibly higher than that between runs adopting different disk inclinations; indeed inclination effects are appreciable only when extreme cases are compared, namely an edge-on versus a face-on run (where the disk inclination is intended relative to the direction of motion of the background gas flow). We note that for the most massive model, V60c4, we have performed only adiabatic runs since our main goal here is to estimate the maximum amount of mass that can be stripped by ram pressure alone. The difference between runs with and without radiative cooling is smaller in terms of stripping radii than it could be guessed from the difference in the amount of stripped mass (Table 2). The reason is that the distribution of gas in the cooling runs becomes more concentrated (thus a given radius contain more mass) as we noted before.

Our results show that model V28c4 is completely stripped in all cases (e.g. Figure 9) except when cooling and an inclination of 90 degrees with respect to the flow are used

at the same time (both choices go in the direction of minimizing stripping). Instead the models V60c4 and V40c20 always retain a significant amount of gas. This indicates that if the progenitors of dSphs once had massive halos corresponding to $V_{peak} \sim 50$ km/s, as suggested by recent cosmological simulations (Kravtsov, Gnedin & Klypin 2004), ram pressure alone was not able to remove their gas early on unless the halo density was once significantly higher than 10^{-4} atoms cm $^{-3}$. On the other end, these results also suggest that efficient gas removal from ram pressure could have happened at some later stage if tides were able to weaken the potential well of the dwarf bringing V_{peak} down to ~ 30 km/s. Interestingly, an NFW halo with $V_{peak} \sim 30$ km/s or lower does fit the present-day velocity dispersion of dSphs (Lokas 2002; Kazantzidis et al. 2004). We will come back to this in the following sections

We tried to compare our numerical results with simple analytical estimates of the effectiveness of ram pressure

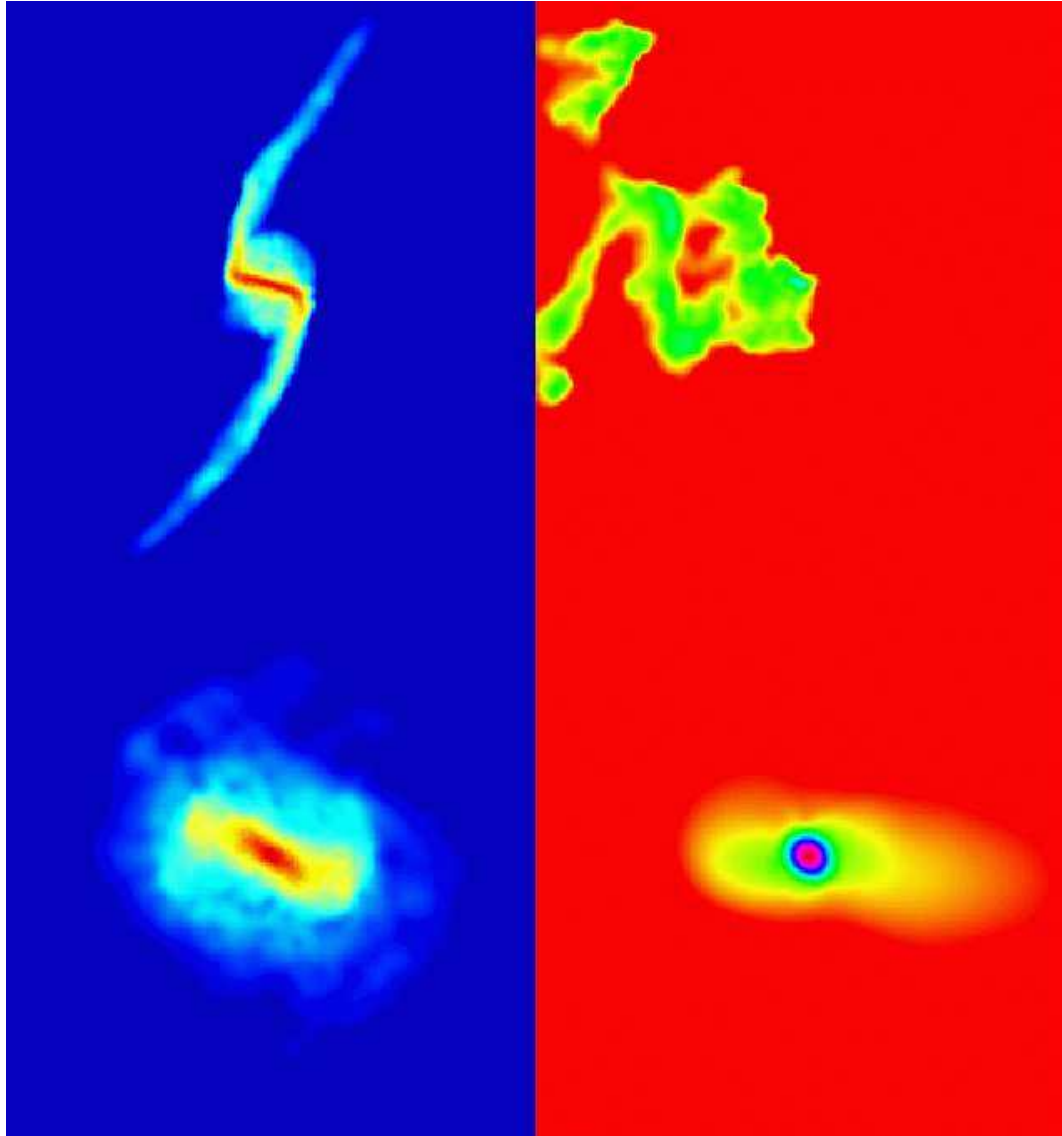


Figure 5. Color coded gas density (right) and stellar logarithmic density maps (left) for run Rc4bRC. Projections along the orbital plane are shown in a box of 30 kpc on a side at $T = 1.7$ Gyr (top) and in a box of 10 kpc on a side at $t = 6$ Gyr (bottom) after the second pericenter passage. All boxes are centered on the center of mass of the bound stars. Re-accretion of gas between the two different times has clearly occurred (the gas distribution is completely displaced from the stars at $T = 1.7$ Gyr).

stripping. Gas is removed from the disk of the dwarfs if the ram pressure force is greater than the restoring force per unit area provided by the disk and halo of the dwarf. The condition for ram pressure stripping for an axisymmetric disk system is expressed by (Gunn & Gott 1972)

$$\rho_h v^2 > 2\pi G \Sigma(R) \Sigma_g(R), \quad (2)$$

where v is the velocity of the galaxy with respect to the surrounding medium, ρ_h is the density of the hot halo of the MW and $\Sigma_g(r)$ is the cold gas surface density at the radius R . Σ represents the surface mass density of the disk. The minimum radius given by Equation (2) is the final stripping radius R_{str} beyond which the ISM can be removed from the galaxy. Equation (2), however, neglects the contribution from dark matter to the restoring force (see Gavazzi et al. 2001). In all of our models the dark matter content is high even near the disk; we will simply account for that by replac-

ing $\Sigma(R)$ with $\Sigma_{dm} + \Sigma_b(R)$, where Σ_{dm} is the surface mass density of the dark matter in a slab with height comparable to the disk thickness and $\Sigma_b(R)$ is the surface mass density of the baryons within the same slab (in our models the gas component always gives a non negligible contribution to the disk mass). This formula describes the instantaneous stripping of gas. We found it difficult to use this prescription as to reflect both the complex interplay between mechanical and thermodynamical effects seen in the simulations and the fact that the stripping is not exactly instantaneous but continues for some time (typically it saturates after ~ 0.2 Gyr). In particular, $\Sigma_g(r)$ is strongly time dependent due to the action of heating and cooling as we noted above. We find that a reasonable prediction can be obtained if we choose not the initial $\Sigma_g(r)$ but that at the time the gas begins to heat up (as little as 10^6 years after the beginning of the simulations). The predicted stripping radius (see Table 2)

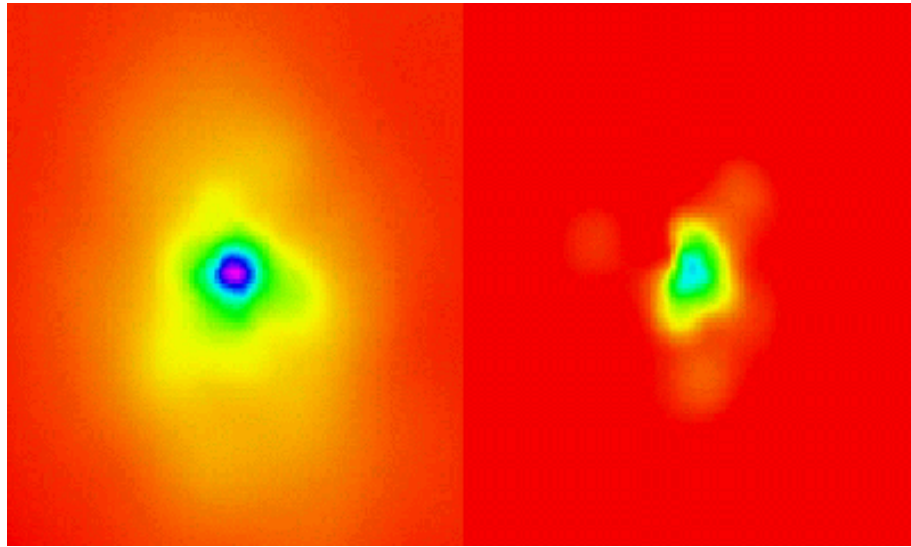


Figure 6. Color coded logarithmic gas density maps for run Rc20RC (left) and for run Rc20RCUV (right) at $t = 5$ Gyr, after three pericenter passages. The projection along the orbital plane is shown. The boxes are 10 kpc on a side and are centered on the center of mass of the bound stars. Clearly the gas remaining in the dwarf is much less and much more diffuse when UV heating is added.

can be slightly larger than that in the simulations (even for runs with cooling). However, the prediction is always close to the stripping radius measured in the simulations at earlier times, i.e. when the approximation of a single, instantaneous stripping event is better satisfied.

3.1.2 Full Interaction (FI) runs

In these runs the dwarf galaxy evolves under the combined action of tides and ram pressure. The mass loss as a function of time for a number of runs is shown in Figure 13. At any given time we identify as bound to the dwarf the gas with temperature $T < T_{vir}$ (where T_{vir} is the initial virial temperature of the halo of the dwarf, in the range $\sim 3 \times 10^4 - 10^5 K$ depending on the model) and which is located within the bound stellar component. We checked that by using this definition one essentially selects the gas that is gravitationally bound to the dwarf.

The angle between the direction of the flow in the hot halo and the plane of the disk is continuously changing because of the orbit of the galaxy and since the disk inclination relative to the orbit changes as the dwarf is tidally torqued by the primary. We compare the gas mass losses observed in FI runs with those occurring in the face-on WT runs which yield the highest possible gas mass loss due to ram pressure only. In general galaxies lose more gas compared to WT runs (compare Table 1 and Table 2 for both adiabatic and cooling runs). However, as we found previously, only in some of the runs (mostly those employing model V28c4) is the dwarf completely stripped of its gas content (see Table 1). Furthermore, while with tides added a dramatic increase in the stripping is always observed in adiabatic runs, stripping can be unexpectedly less effective in cooling runs (compare run Rc4bRC in Table 1 with all the “c4a” runs in Table 2). This happens because the tidally induced bars funnel 20 – 40% of the initial gas content of the disk within a radius smaller than the initial disk scale length of the dwarf. The gas shocks through the bar as it loses angular momentum and heats up.

In adiabatic runs this heat cannot be dissipated quickly and the gas ends up more extended. In cooling runs the gas loses rapidly its thermal energy and there is not enough pressure to stop its inflow. As a result gas profiles become much more concentrated in cooling runs and a larger amount of gas ends up deeper in the potential well where it is harder to strip (Figures 14-15). In runs which include the heating from the UV background the gas remains more extended than with just radiative cooling (Figure 6) and stripping is much more efficient, with gas mass losses closer to those of adiabatic runs.

Despite the complex interplay between bar instability and thermal physics, it turns out that the fractional amount of stripped mass correlates well with the initial V_{peak} of the satellite on a given orbit, both with and without cooling (for example compare run Rc4cRC and run Rc20RC in Table 1, or run Rc4aRCUV and run Rc4bRC). For the same initial V_{peak} , orbits with smaller pericenter lead to a larger reduction in the V_{peak} due to more numerous and stronger tidal shocks (Figure 16). This favours ram pressure stripping as it lowers the gravitational restoring force. Furthermore, on orbits with a pericenter of 30 kpc the maximum halo gas density is about a factor of 3 higher relative to the case with a pericenter of 50 kpc, and this also favours ram pressure stripping. As a consequence gas mass loss is significantly larger and faster in runs using a more plunging orbit (Table 1).

Estimating the stripping radius from formula (2) is somewhat meaningless in these runs because the depth and shape of the potential of the dwarf is continuously changing due to the action of tides and the distribution of the bound gas also changes with time. Nonetheless, it is noteworthy that the stripping radius estimated using formula (2) with the parameters of the initial models is from 2 to 3 times larger than the radius at which most of the bound gas sits in the FI runs after the first pericenter passage, hence after bar formation and inflow. This is because the remaining

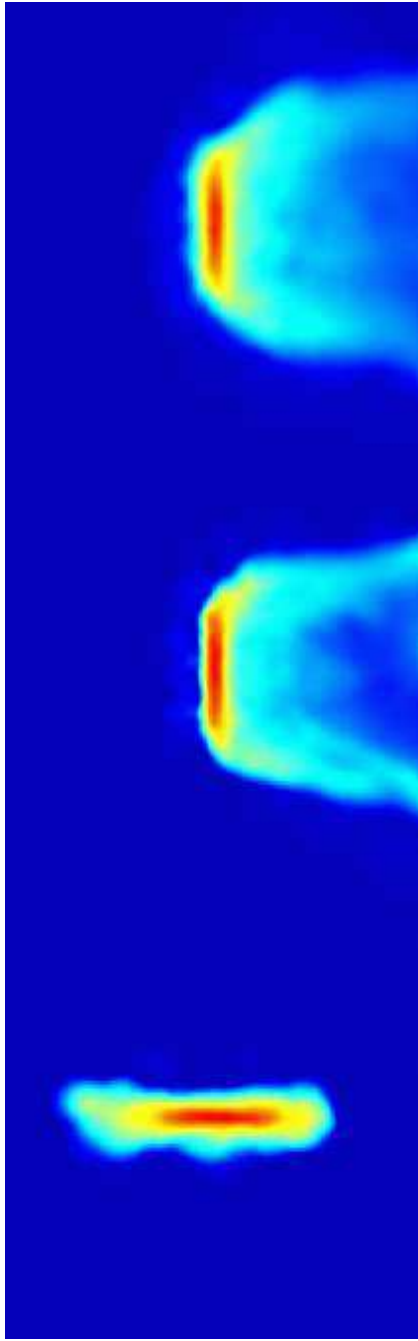


Figure 7. Color coded logarithmic gas density map for three wind tunnel (WT) runs. From top to bottom, an edge-on view after $t = 0.05$ Gyr of the gas disk in runs T1c20, T2c20, T3c20. The background gas flows along the horizontal axis from left to right (from right to left in the bottom panel). Boxes are 10 kpc on a side.

bound gas is that material which flows to the center of the bar.

One interesting feature of cooling runs is that sometimes re-accretion of gas is observed. This is clearly shown by the sequence in Figure 5 (compare the location of the stars and the gas at the two different times) and also shows up in some of the curves of the mass loss (top panel in Figure 13). This happens when gas is stripped from the disk near

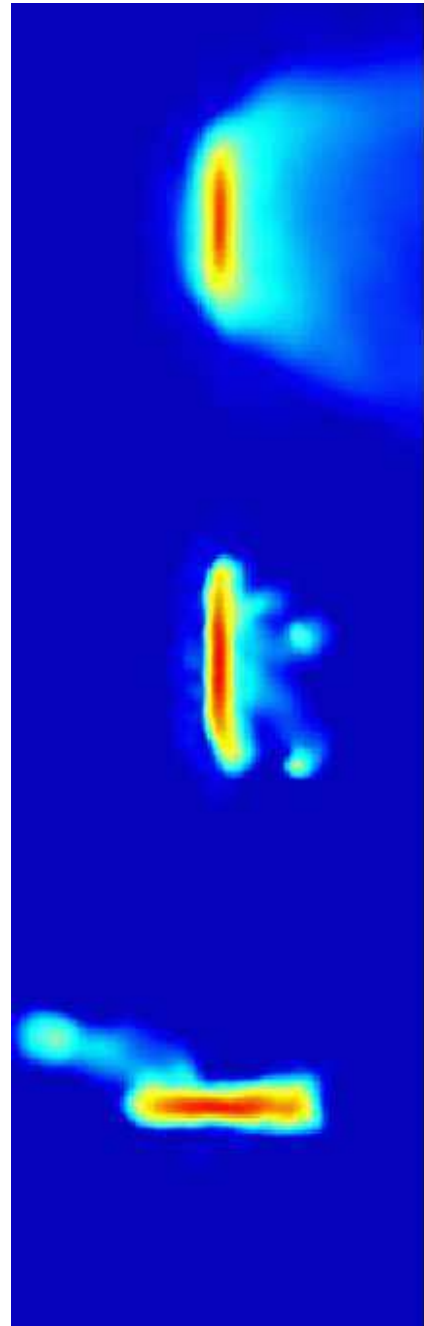


Figure 8. Color coded logarithmic gas density map for three wind tunnel (WT) runs. From top to bottom, an edge-on view after $t = 0.3$ Gyr of the gas disk in runs T1c20, T2c20, T3c20. The background gas flows along the horizontal axis from left to right (from right to left in the bottom panel). Boxes are 10 kpc on a side.

pericenter but does not have enough momentum to escape the galaxy. As the galaxy moves towards apocenter, where relative velocities are lower, the gas falls back onto the disk. This is not observed in adiabatic runs because gas that has been removed from the disk quickly becomes hotter than the virial temperature of the dwarf halo.

We repeated several of these simulations without a gaseous halo to isolate the efficiency of gas removal by tides alone. The amount of gas stripped is a factor of 3 to 6 less

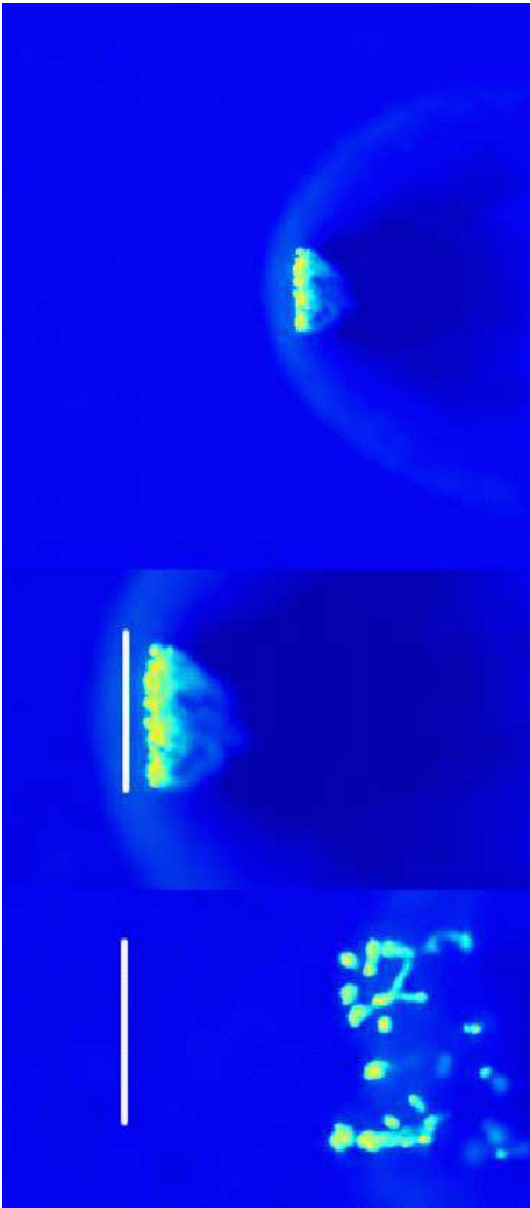


Figure 9. Color coded logarithmic gas density map for the gas of the dwarf in run T2c4b. On top the output after $t = 0.05$ Gyr is shown in a box of 30 kpc on a side. The bow shock is clearly visible. In the middle panel we show a zoom-in of the same snapshot (the box is 10 kpc along the longest axis). The bottom panel shows a zoom-in of a snapshot taken after $t=0.3$ Gyr (the box is also 10 kpc along the longest axis). The white vertical bar shows the location of the stellar disk. Complete gas stripping occurs in this case. The background gas flows along the horizontal axis from left to right.

than the simulations which include ram pressure stripping, depending on the radiative cooling (Figure 13). When compared with the WT runs where only ram pressure is included, tides strip from similar to appreciably lower amounts of mass (lower panel of Figure 13). The relative increase of stripping when ram pressure is added to tides is maximum for model V40c20, that has the steepest rise of the dark matter density in the center (see Figure 1). This reflects the different physical scalings of ram pressure and tidal

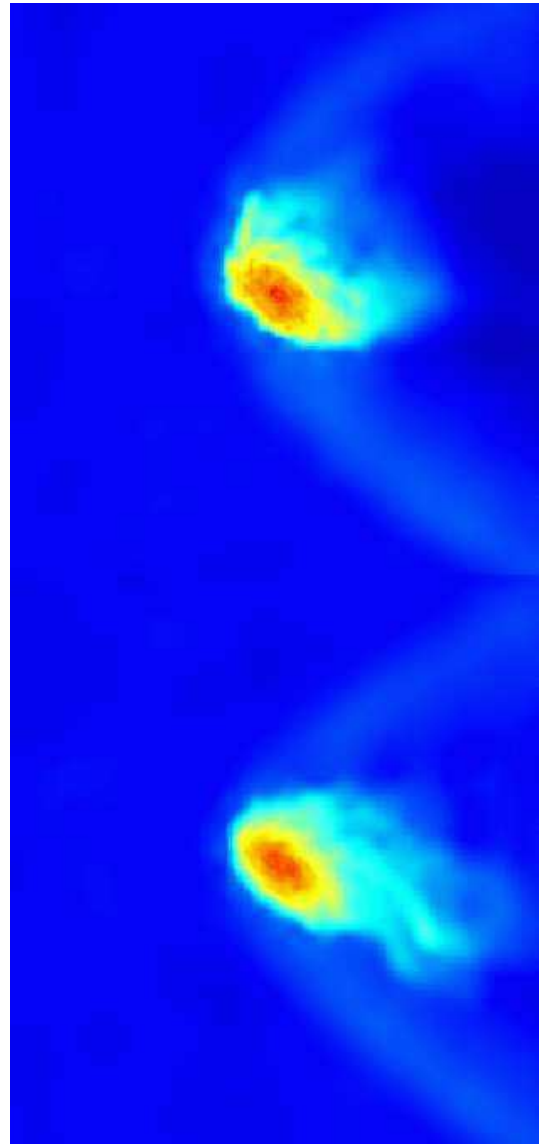


Figure 10. Color coded logarithmic gas density map for the gas of the dwarf in run T2c4b. From top to bottom, the outputs after $t = 0.05$ Gyr and $T = 0.3$ Gyr are shown. The boxes are 30 kpc on a side. The background flow is along the horizontal axis from left to right.

forces. In these highly concentrated halos the response to tidal shocks is nearly adiabatic near the center (Taffoni et al. 2003; Kazantzidis et al. 2004), hence stripping is expected to be minimal inside $R_{v=v_{peak}}$. However, this is applicable only to stripping induced by tidal shocks; the timescale on which instantaneous ram pressure acts is instead much smaller than that of tidal shocks, $< 10^7$ years (we follow Mori & Burkert 2000 for parameters of e.g. run Rc20V60RC) against $\sim 10^8$ years ($\sim R_{peri}/V_{peri}$). Such timescale is also smaller than the local gas orbital time even in a highly concentrated halo ($> 10^7$ years) hence the response of the galaxy to ram pressure is impulsive instead of adiabatic. On the other end, the other models, having low concentration haloes, respond more impulsively to tides in the first place, so that the increase in stripping efficiency is not so dramatic.

In these simulations the peak velocity of the rotation

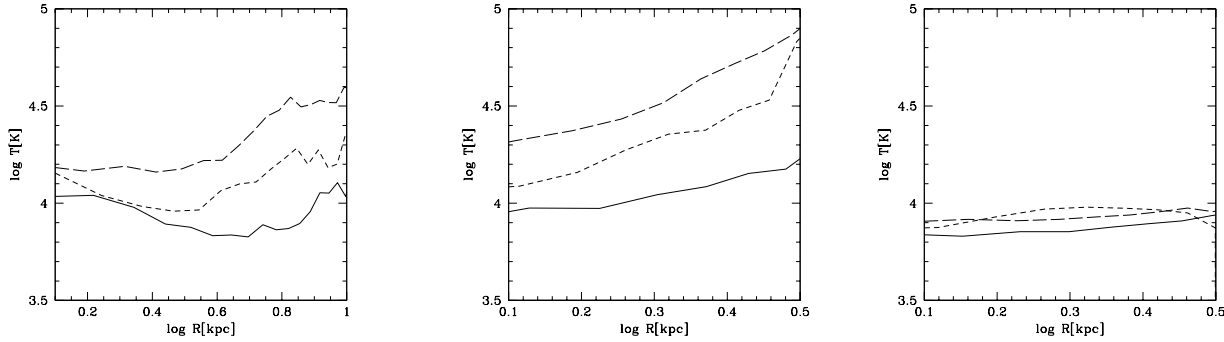


Figure 11. Evolution of temperature profiles of the gas in WT runs. Profiles are azimuthally averaged in a cylinder with height twice that of the stellar disk (R is the cylindrical radius). The solid line is for $t = 0.02$ Gyr, the short-dashed line for $t = 0.1$ Gyr and the long-dashed line for $t = 0.3$ Gyr. From left to right, run T1c4b, T1c20 and T2c20 are shown

curve of the satellites, V_{peak} , drops by 20 – 50% after several orbits (Figure 16) while in cosmological simulations it often decreases by more than a factor of 2 over several Gyr (Kravtsov et al. 2004, but see Ghigna et al. 1998). Such difference may be due to the limited number of orbital configurations here explored (some of the satellites in Kravtsov et al. (2004) have pericenters even smaller than 30 kpc) and/or to the fact that cosmological runs do not include baryons and do not have enough force and mass resolution to follow the complex disk evolution, especially bar formation and the resulting gas inflows that can produce a remarkable increase in the central density (our force resolution is 5 times better than the best published cosmological simulations with baryons). These issues will be investigated systematically in a forthcoming paper (Kazantzidis, Mayer et al., in preparation).

In summary, the final gas fractions drops to 0 – 50 % of the initial gas content for galaxies on orbits with pericenter of 50 kpc, with 10% being a typical fraction, and to as low as 0 – 6 % of the initial values for galaxies on an orbit with pericenter of 30 kpc (see Table 1). In the runs that include the effect of the cosmic UV background even when there is gas left inside the dwarf this is ionized, and the observational upper limit on the mass of neutral hydrogen in dSphs, $M_{HI} < 0.01 M_s$, where M_s is the stellar mass, is fully satisfied. The gas will be able to recombine later on as the cosmic background fades away, but the local ultraviolet radiation flux from the Milky Way or M31 might be enough to keep it ionized even at low redshift (Maschenko, Carignan & Bouchard 2004). The current upper limits on the total amount of gas in dSphs including the ionized component, are much higher, $M_g < 0.1 M_s$ (Gallagher et al. 2003) , and are satisfied in the final states of the dwarfs for the majority of our runs. Hence a combination of ram pressure and tidal stripping succeeds in explaining how dwarf spheroidals have little or no neutral hydrogen today. On any given orbit, dwarf models with higher V_{peak} are stripped less severely and, in particular, our most massive model, V60c4, ($V_{peak} = 62$ km/s), always retains a substantial amount of gas. This is consistent with the fact that bright dwarf elliptical (dEs) satellites of M31, like NGC205, whose central

velocity dispersion, $\sigma = 30 – 45$ km/s, is comparable to that of the evolved states of model V60c4, do have some amount of neutral gas (Mateo 1998).

When neutral gas remains in the dwarfs, most of it will be rapidly turned into stars as it reaches very high densities due to the effect of the bar, and bursts localized near the center of the dwarf are expected at pericenter passages. as described in Mayer et al. (2001a). Hence we predict that the higher the mass of the dwarf (not its luminosity) the more extended its star formation history should be. For dwarfs that start out with similar masses, our simulations suggest that the outcome will vary depending on their orbit. A signature in the star formation history of the dwarfs is expected at the epoch when it underwent the first close approach within the Milky Way. This can be either a burst or a marked depression of the star formation depending on whether just a fraction or most of the gas is removed from the dwarf galaxy.

3.2 Kelvin-Helmholtz instabilities and turbulent stripping

Gas that survives instantaneous ram pressure can be stripped by the Kelvin-Helmholtz (KH) instability developing at the interface between the gas of the dwarf galaxy and the ISM (Nulsen 1982; Murray et al. 1993, Quilis et al. 2000). This is also known as turbulent stripping since the gas reaches a turbulent state as the instability develops. In order to develop KH instabilities require a sharp boundary to exist between the two fluids. Even at the high resolution adopted here SPH is hardly capable of resolving KH instabilities mostly because the artificial viscosity and the fact that densities are smoothed in SPH both contribute to “blur” any sharp interface. An approximate “effective” local kinematical viscosity can be calculated as $\nu = \alpha c_s h/8$, where α is the coefficient of the linear term in the artificial viscosity, c_s is the sound speed and h is the SPH smoothing length (Lufkin et al. 2004). The Reynolds number is then $Re \sim Lv_{gal}/\nu$, where L is the typical size of the object moving in an external medium (the disk of the dwarf here) and v_{gal} is the speed

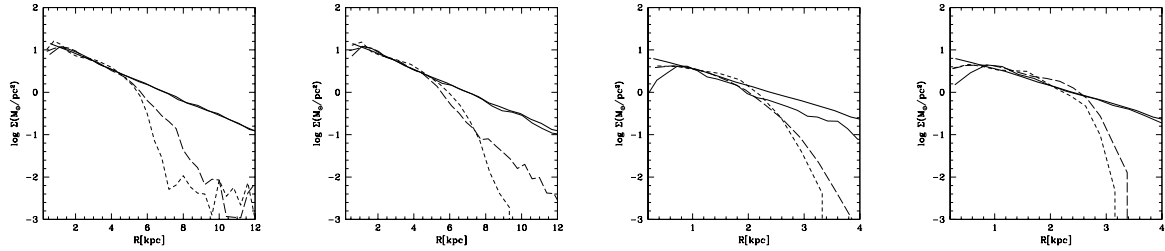


Figure 12. Evolution of density profiles of the gas in WT runs. Profiles are azimuthally averaged in a cylinder with height equal to that of the stellar disk (R is the cylindrical radius). The thick solid line is for $t = 0$, the thin solid line for $t = 0.02$ Gyr, the short-dashed line for $t = 0.1$ Gyr and the long-dashed line for $t = 0.3$ Gyr. From left to right, runs T1c4b, T3c4b, T1c20 and T2c20 are shown

at which it is moving; this number is strictly a function of position (since ν is a function of position) and is in the range $20 - 100$ in our runs (the highest Reynolds numbers occur in the highest resolution WT runs). This is of course much lower than the Reynolds numbers typical of turbulent flows (up to 10^4). Aside from numerical issues that might hamper the development of KH instabilities in the simulations we can ask whether turbulent stripping is likely to be important for dwarf galaxies moving in a very diffuse halo as those that we are modeling here. Mori & Burkert (2000) found that spherical dwarf galaxies moving at a few thousand km/s in a dense cluster hot halo will be stripped on a timescale significantly smaller than the crossing time of the galaxy in the cluster. Following Mori & Burkert (2000) we use the following equation to obtain an estimate of the expected characteristic timescale for stripping by KH instabilities including the stabilizing effect of gravity (which is mainly provided by the dark halo potential in our models);

$$\tau_{\text{KH}} = \frac{FM_0}{M_{\text{KH}}}, \quad (3)$$

$$= 2.19 \times 10^9 \left(\frac{F}{0.1} \right) \left(\frac{M_0}{10^9 M_{\odot}} \right)^{\frac{1}{7}} \left(\frac{n_h}{10^{-4} \text{cm}^{-3}} \right)^{-1} \times \left(\frac{v_{\text{gal}}}{10^3 \text{km s}^{-1}} \right)^{-1} \text{yr.} \quad (4)$$

The equation assumes spherical symmetry, which is a reasonable assumption since our galaxies are dominated by a spherical dark matter halo. In the equation M_0 is the CDM halo mass within the radius R_{strip} down to which galaxies are stripped in the WT runs (see Table 2, these simulations offer a cleaner test case since they include only ram pressure), $F = M_{\text{bar}}/M_0$ is the mass ratio between the baryons and the CDM halo within the same radius, and $\dot{M}_{\text{KH}} = \pi R_{\text{strip}}^2 \rho_h v_{\text{gal}}$ is the mass loss rate from the galaxy through KH instabilities (ρ_h is the hot halo density and v_{gal} is the velocity of the galaxy through the hot halo). For the gas densities ($\sim 10^{-4}$ atoms cm^{-3}) and velocities occurring at pericenter the timescale for KH stripping is, respectively, 4 Gyr for model V40c20 and 10 Gyr for model V60c4, these being the model galaxies in which instantaneous ram pressure is not capable of removing all the gas. For the gas densities and velocities where the satellites spend most of their time, namely at distances larger than 100 kpc, the KH stripping timescale is at least several Hubble times.

Shear viscosity in a laminar flow ($Re < 30$) can also produce a slow stripping of the gas with timescales and mass loss rates comparable to those of KH stripping in the turbulent regime (Nulsen 1982). Physical viscosity is not included in our treatment of SPH and therefore this viscous stripping mode is missing. Spurious viscous stripping from the artificial viscosity term is limited by our reasonably high resolution and the Balsara correction. The characteristic viscous time is $\tau = L^2/\nu \approx 10$ Gyr, which means viscosity effects are negligible given that the important timescales, those related to ram pressure and tidal shocks, are much smaller (between 10^7 and 10^8 years). Tittley, Pearce & Couchman (2001) have shown that SPH can alter the magnitude and scaling with density of hydrodynamical drags because of the way pressure forces among neighboring cold and hot background particles are calculated (in essence the cross section of an object moving in a hot medium can be artificially enhanced or decreased). However, the effect is particularly severe, enhancing the drag over the expected value, only in the subsonic regime, whereas our galaxies all move at slightly supersonic velocities.

In summary, our simulations have enough resolution to overcome artificial viscous stripping but cannot model correctly turbulent stripping yet. However, although SPH is often blamed for its inability to model hydrodynamical turbulence we recall that published grid simulations are of similar quality when it comes to the ability to model turbulence – Marcolini et al. (2003) find Reynolds numbers similar to what we find.

3.3 Dark and baryonic contents of the remnants: can we explain Draco?

In FI runs the stellar disk is stripped and transformed into a spheroidal system by means of tidal heating and barbuckling instabilities as described in Mayer et al. 2001a,b. The ratio $M_{\text{dark}}/M_{\text{bar}}$ between dark matter mass and baryonic mass in the final objects varies between 3 and 12, the highest values occurring in runs with model V40c20. In remnants with the highest dark matter contents or highest central concentration of gas the buckling instability is weaker, with the result that the bar-like shape is preserved. The trend with gas concentration is consistent with the findings of Debattista, Mayer et al. (in preparation) for isolated bar-unstable galaxies with gas. However, in reality the central

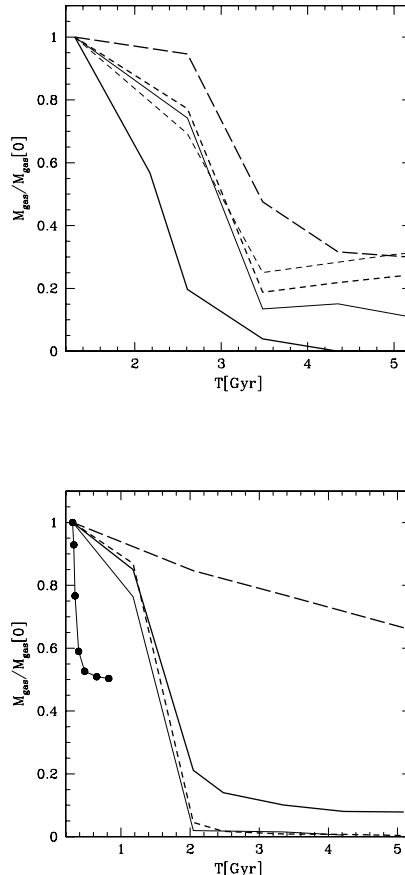


Figure 13. Time evolution of the bound gas mass for FI runs using model V60c4, V28c4 (top) and runs using model V40c20 (bottom). Top: run Rc4aAD (thin solid line), Rc4aRCUV (thin short-dashed line), Rc4bTD (long-dashed line), Rc4bAD (thick solid line), Rc4bRC (thick short-dashed line). Bottom: run Rc20TD (long dashed line), Rc20AD (thin solid line), Rc20RC (thick solid line), Rc20RCUV (short dashed line). The line with dots shows the mass loss rate (due to ram pressure only) for one of the WT runs, T1c20 (see Table 2 – the curve stops at less than 1 Gyr since WT runs were run for a short timescale since stripping saturates very early on).

gas would form stars and its distribution will become less concentrated. The final central v/σ of the stars is below 0.5, thus compatible with those of dSphs, and the central final velocity dispersions are in the range 10 – 30 km/s.

We can ask whether the remnants of model V40c20, can reproduce the overall properties of Draco, one of the most extreme dSphs in terms of low luminosity and high M/L . In adiabatic runs the gas is completely stripped after the first pericenter passage. The observed truncation of the star formation history in Draco could be thus interpreted as the result of its infall into the Milky Way halo. However, in runs with cooling some gas is retained. Assuming a star formation rate comparable to that deduced for Draco and Ursa Minor by Hernandez et al. (2000), $100 - 200 M_{\odot}/\text{Myr}$, we obtain that the remaining gas in run Rc20RC will be turned into stars in about 5 Gyr, leaving a dwarf completely devoid of gas. But this implies a fairly extended star formation history, contrary to what observed for Draco, and the amount of gas that needs to be turned into stars is non-negligible, $\sim 6 \times 10^6 M_{\odot}$; if we sum such mass to the remaining bound stellar mass we get $5 \times 10^7 M_{\odot}$. For a mass-to-light ratio ~ 4 , as typical of old stellar populations we would get a

luminosity $\sim 10^7 M_{\odot}$, i.e. 50 times higher than the V band luminosity of Draco (Odenkirchen et al. 2001). Since the largest fraction of the final baryonic mass is contributed by the initial stellar mass in the model (tidal stripping is moderate in highly concentrated haloes) an excessive final luminosity would result also in adiabatic runs. As for the dark matter content one would obtain $M/L = \sim 50$, as high as typical estimates for M/L in Ursa Minor and comparable to the lower limits for M/L in Draco (Mateo 1998; Wilkinson et al. 2004). The final projected central velocity dispersion, ~ 15 km/s, is consistent with the peak velocity dispersion of Draco (Wilkinson et al. 2004). The central dark matter density measured for the stirred dwarf at the end of the simulation, $0.065 M_{\odot}/pc^3$ is also in rough agreement with the value estimated for Draco ($\sim 0.1 M_{\odot}/pc^3$). Thus run Rc20RC produces a model with roughly the right dark matter content but an excessive baryonic content. Adding heating and photoionization from a uniform UV background (run Rc20RCUV) aids gas removal and leaves essentially no neutral gas after a few Gyr. In this case the star formation history, as in the adiabatic runs, would have been essentially truncated after the first close encounter with the Milky Way.

Nevertheless, the total stellar mass of the dwarf would still yield a luminosity about an order of magnitude higher than that of Draco.

The final luminosity depends on the initial stellar and gas content of the model, which was chosen to be fairly representative of the baryonic content of today's dIrrs. Although Draco likely had a halo massive enough to resist gas removal from supernovae feedback or photoionization, the progenitors from which it assembled at very high redshift were certainly much smaller and were likely affected by these mechanisms. Hence one can imagine that the main progenitor of Draco had a baryon fraction much lower the one we used here. In such a scenario, however, environmental effects would not have played the primary role in setting the current high M/L of Draco. One alternative explanation is to imagine that Draco was a mostly gaseous disk dwarf by the time it entered the Milky Way, with minimal star formation having taken place. Such a low star formation rate can be simply the result of an extended, relatively high angular momentum disk being almost everywhere Toomre stable and below the density threshold necessary for star formation to happen, as observed today in some dIrrs and LSB galaxies (Verde, Oh & Jimenez 2002). To explore this possibility we have run a simulation in which the initial model has the same structural properties of model V40c20 except that now as much as 90% of the disk is gaseous. A weaker stellar bar forms given the lower stellar mass which produces a weaker gas inflow, and a larger relative fraction of the disk mass is stripped by ram pressure. In an adiabatic run all the gas is stripped after two pericenter passages, leaving a gas-free remnant that roughly matches the luminosity of Draco after ~ 3 Gyr. In a run with cooling and the cosmic UV radiation of order $10^5 M_\odot$ of gas remain in the dwarf, but all this gas is ionized and no star formation would be possible, and even in this case the final stellar mass would be comparable to that of Draco.

3.4 Fate of stripped gas

The stripped gas has a very different fate in the adiabatic and in the cooling runs. In the adiabatic runs it ends up quite diffuse and hot ($T > 10^5$ K) and quickly thermalizes and mixes with the gas in the MW halo. When cooling is allowed the gas along the tails fragments into dense clouds and sheet-like structures pressure confined by the ambient medium. This is shown in Figure 17. These clouds remain cold ($T < 10^5$ K) until they are dissolved as they sink deeper in the potential well due to gas drag. Sinking of the gaseous tails is marginal in the adiabatic runs because the stripped gas is too diffuse to experience significant drag. Fragmentation is suppressed in the first place in adiabatic runs because the density of the gas along the tails is too low for the cloud to reach pressure equilibrium within the hot ambient medium. In the simulations with UV heating, clouds are also present, although they are slightly more diffuse and hotter (see Figure 17).

Individual clouds survive for a timescale of $\sim 10^8$ years. The dissolution of the clouds is due to a combination of ram pressure and tidal disruption, but spurious evaporation due to artificial viscosity and discreteness effects (particle-particle collisions) may be important, especially for the smallest clouds that are close to the resolution limit (we

consider a cloud to be unresolved if it contains less than 64 particles, i.e. twice the number of neighboring particles used in the SPH calculation). We calculate that ablation of the clouds due to Kelvin-Helmoltz stripping would occur on timescales comparable to the dissolution timescales observed in the simulations.

A single stripped satellite produces tens of blobs with masses in the range $10^4 - 10^6 M_\odot$ and sizes in the range 0.5 – 5 kpc. These blobs could explain the cold HI fragments identified by Thilker et al. (2004) around M31. These clouds have column densities ($\sim 10^{20}$ cm $^{-2}$) and masses (if placed at roughly the distance of M31) of $10^5 - 10^6 M_\odot$, similar to the most massive among our clouds. They have different velocities with respect to the systemic velocities, which lead Thilker et al. to suggest that they could hardly be tidal debris of disrupted dwarfs. However, a spread in velocities arises naturally because of the drag exerted by the diffuse gaseous halo. We measure velocities differing by up to a factor of 2 among the clouds in our simulations. The variety of shapes of the clouds detected by Thilker et al. ,from nearly spherical to elongated filaments, is also reproduced by our simulations (Figure 17). The clouds do not appear tidally disturbed because they are pressure confined. However, their origin is partly tidal since they are the result of the combined removal of gas by tides and ram pressure. Although our simulations lack low temperature cooling (by molecules and metals) the heating from the cosmic or local UV radiation should keep their temperature and densities close to the values observed in the simulations. However, since many of the clouds are just above our resolution limit we feel that it is premature to draw firm conclusions concerning their structure. Nonetheless the simulations strongly suggest a connection with HI fragments and possibly other gaseous structures observed in the Local Group like some of the high velocity clouds (HVCs) and the Magellanic Stream (see also Mastropietro et al. 2004).

4 SUMMARY AND CONCLUSIONS

The combination of ram pressure and tidal forces can produce systems resembling gas poor dwarf spheroidals from disk-like progenitors. Here we summarize our findings:

- Ram pressure alone can remove completely the gas only in dwarfs having halos with $V_{peak} \lesssim 30$ km/s. This is consistent with the results found by Marcolini et al. (2003) using different initial conditions and a different numerical technique.
- Compressional heating arising as the dwarf travels through the outer medium can significantly enhance ram pressure stripping by producing a more extended gas distribution. As a result, stripping is more effective in adiabatic runs than in cooling runs since in the latter such heating is dissipated.
- The combination of tides and ram pressure is in general more effective at removing gas from the dwarfs than ram pressure alone and always significantly more effective than tides alone. Tidal stripping lowers V_{peak} and thus the depth of the potential well of the dwarf.
- Tidally induced bar formation opposes ram pressure stripping by driving a large fraction of gas towards the center where it is harder to strip at subsequent pericenter passages.

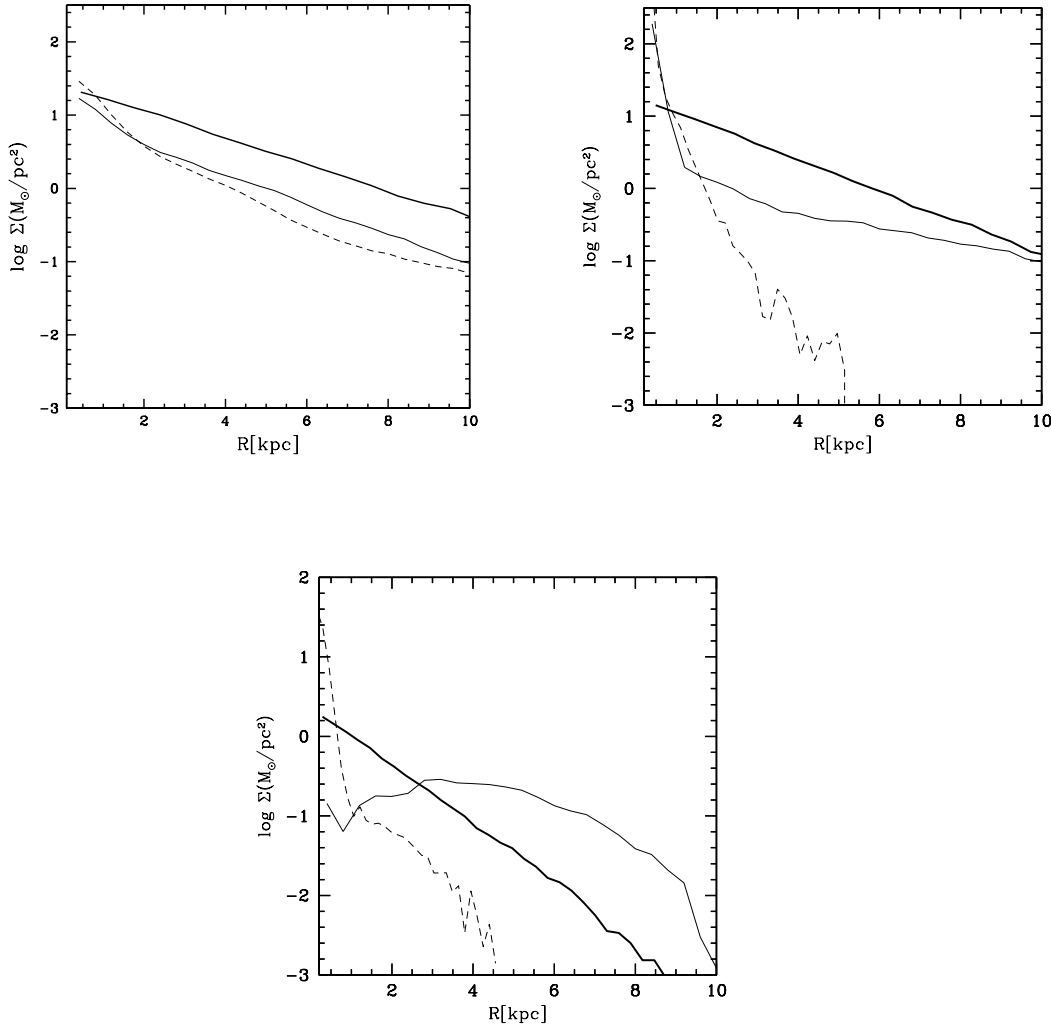


Figure 14. Evolution of gas surface density profiles in FI runs. The thick solid line is used for the initial profile, the thin solid line is used for the profile at $T=3$ Gyr (after first pericenter passage), and the dashed line is used for the profile at $T=6$ Gyr (after second pericenter passage). From top left to bottom, the runs Rc4aAD, Rc4aRCUV, and Rc4bRC are shown. The unusual shape of the profile at intermediate times in the bottom panel reflects the fact that gas is displaced from the galaxy at this point (see also Figure 5).

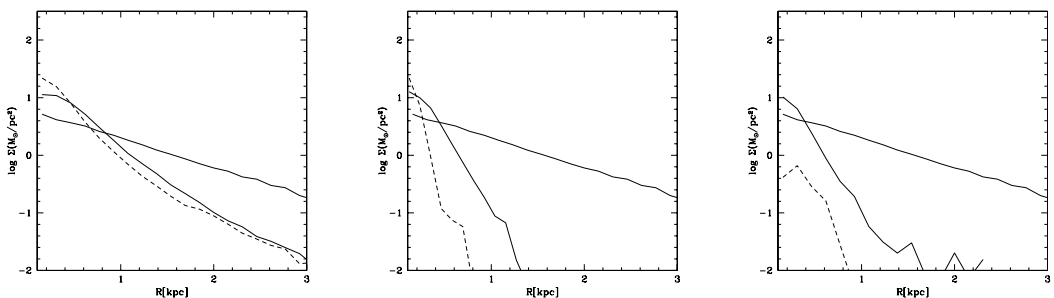


Figure 15. Evolution of gas surface density profiles in FI runs. The thick solid line is used for the initial profile, the thin solid line for the profile after first pericenter crossing ($T=1$ Gyr) and the dashed line for the profile after second pericenter passage ($T=3$ Gyr). From left to right, run Rc20TD, Rc20RC, and RC20RCUV are shown.

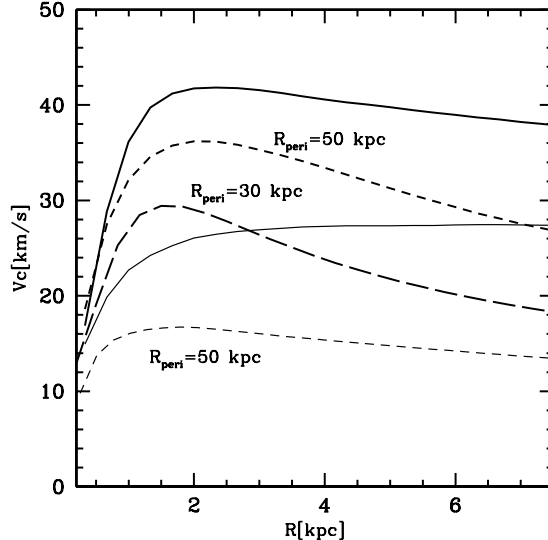


Figure 16. Evolution of the rotation curves of the dwarfs (including the contributions of both dark matter and baryons) in run Rc20TD (thick lines) and run Rc4aTD (thin lines). The solid lines represent the initial conditions while the short-dashed show the curves after 3 orbits, corresponding to $t = 4$ Gyr and $t = 10.2$ Gyr, respectively. The thick long-dashed line shows the curve for run Rc20bAD after $t = 10.2$ Gyr. Pericenter distances for the various orbits are indicated in the plot. Note that runs Rc20TD and runs Rc20bAD employ the same initial dwarf model but different orbits.

This counteracting effect is stronger when radiative cooling is included and explains why in a few cases the addition of tides does not increase the amount of stripped mass.

- Low baryonic contents and high mass-to-light ratios comparable to those of many dSphs can be obtained as a result of ram pressure and tidal stripping. However heating sources, such as the cosmic UV background arising during reionization, are required in order to obtain a very low gas fraction in a halo as massive as that in which Draco is probably embedded.

- The gaseous stream produced by the stripped dwarfs fragments into several cold clouds pressure confined by the outer medium. These clouds have properties reminiscent of gaseous structures possibly associated with the Local Group, including some of the HVCs and the HI fragments recently detected around M31.

We have considered only two types of orbits in this paper. Since proper motions of dSphs are poorly constrained (recent HST-based measurement still have a quite large error, e.g. see Piatek et al. 2003 for Carina) there is still quite some freedom in choosing the initial orbits. For example evolving model V40c20 on an orbit with smaller pericenter, say between 10 and 20 kpc, would enhance both tidal stripping and ram pressure. More eccentric orbits would lead to higher pericentric velocities which greatly increases the efficiency of ram pressure stripping. Furthermore, the progenitors of dSphs might have suffered both tidal and ram pressure stripping already before entering the Milky Way halo (Kravtsov et al. 2004). Hence our results should be regarded as quite conservative.

As we noted above, the initial orbits and initial masses of the dwarfs are both factors that determine the final dark-to-baryonic mass ratio and other properties of the remnants. Therefore, the fact that Fornax and Draco have similar masses, as inferred from their velocity dispersions (Kazantzidis et al. 2004), but differ by more than a factor of 10 in their luminosity, can be explained in two ways. Either the progenitors of these two dwarfs started out with very different relative amounts of dark matter and baryons, for reasons related to their formation history and not to the environment, or they descend from very similar progenitors having comparable dark and baryonic masses, but evolved differently because they entered the primary halo at a different epoch and on different orbits. The ionizing radiation at high redshift also plays a role in determining the efficiency of ram pressure stripping, and its effect again will be stronger for dwarfs infalling at higher redshift. It is a natural consequence of structure formation in hierarchical models that subhaloes that are found closer to the center of the primary system at $z = 0$ are typically those that fell earlier into the potential well of the primary system. Based on their current distances one would conclude, for example, that Fornax is likely a more recent addition to the Milky Way system, and would have suffered fewer and weaker pericenter passages, relative to Draco. It retained some gas after the first one or two orbits, a condition usually satisfied in those of our simulations that have the largest pericenter, and underwent a few bursts over the past few Gyr (Mayer et al. 2001b). Instead, Draco entered earlier on a tighter orbit and lost almost all its gas at the first pericenter passage, thus ending star formation early. We note that for the orbits with a pericenter

of 30 kpc pericenter crossing occurs 0.7 Gyr after the dwarf enters the Milky Way halo. If the dwarf begins its infall at $z = 6 - 7$, i.e. ~ 1 Gyr after the Big Bang, this leaves about ~ 2 Gyr to form stars before gas removal occurs, consistent with the estimated time span for the star formation history of Draco (Grebel & Gallagher 2004). While the infall time of the progenitor of Draco is clearly a free parameter, our results show that these simple assumptions produce a scenario that fits a number of observational constraints.

It is important to keep in mind that the Milky Way halo model used here is based on data at $z = 0$ and the components that we assumed as fixed do indeed evolve through cosmic time. At high z , as the dwarfs began their route towards the Milky Way, the dark halo and gaseous halo masses may have been quite different. However, Λ CDM galaxy formation simulations suggest that large disk galaxies had the last major merger quite early on in order for a large enough disk to assemble by $z = 0$, which means most of the dark halo mass was probably already in place at $z = 2 - 3$. The evolution of the gaseous halo in Λ CDM simulations has not been investigated yet but work in progress suggests its density at several tens of kiloparsecs could have been ten times higher than the value adopted in this paper.

In our simulations ram pressure stripping is most effective close to pericentric passages. This reflects the fact that we have assumed a smooth density distribution for the hot halo. If the halo has a complex multiphase structure as predicted by some models (Maller & Bullock 2004) the dwarfs would move through a clumpy medium and could undergo intense ram pressure stripping even far from pericenter if they encounter a dense and massive cloud. Galaxy formation simulations which follow the build-up and evolution of the gaseous halo at very high resolution with a proper treatment of the multi-phase ISM will eventually be able to address this aspect. However, current cosmological simulations can hardly capture the effect of ram pressure on satellite galaxies even in the case of a smooth halo because of the limited resolution and owing to uncertainties in the star formation and feedback processes which concur to determine the gas fraction in satellite galaxies. Therefore nowadays simulations such as those discussed in this paper represent a necessary counterpart to cosmological runs and provide the only means to test the physical effect of environmental mechanisms in a robust way.

The numerical simulations were carried out on the zBox supercomputer at the University of Zurich and on LeMieux at the Pittsburgh Supercomputing Center.

REFERENCES

Abadi, M. G., Moore, B., Bower, R. G. 1999, MNRAS, 308, 947
 Balsara, D.S., 1995, J. Comp. Phys., 121, 357
 Barkana, R., & Loeb, A., 1999, ApJ, 523, 54
 Benson, A. J., Lacey, C.G., Baugh, C.M., Cole, S., Frenk, C.S. 2002a, MNRAS, 333, 156B
 Benson, A. J., Frenk, C.S., Lacey, C.G., Baugh, C.M., & Cole, S. 2002b, MNRAS, 333, 177B
 Blitz, L., Robishaw, T. 2000, ApJ, 541, 675
 Braun, R., Thilker, D. A. 2004, A&A, 417, 421
 Bullock, J.S., Kravtsov, A.V., & Weinberg, D.H., 2000, ApJ, 539, 517
 Bullock, J. S., Kolatt, T.S., Sigad, Y., Somerville, R.S., Kravtsov, A.V., Klypin, A.A., Primack, J.R., Dekel, A. 2001, MNRAS, 321, 559
 Colpi, M., Mayer, L., Governato, F. 1999, ApJ, 525, 720
 Cowie, L. L., McKee, C. F. 1977, ApJ, 211, 135
 de Blok, W.J.G., & McGaugh, S.S., 1997, MNRAS, 290, 533
 Dekel, A., Silk, J., 1986, ApJ, 303, 39
 Einasto, J., Saar, E., Kaasik, A., & Chemin, A.D., 1974, Nature, 252, 111
 Faber, S.M., & Lin, D.C.N., 1983, 266, L17
 Ferguson, H.C., & Binggeli, B., 1994, A&A Rev, 6, 57
 Ferrara, A., & Tolstoy, E., 2000, MNRAS, 313, 291
 Gallagher, J.S., Madsen, G.J., Reynolds, R.J., Grebel, E.K., & Smecker-Hane, T.A., ApJ, 2003, 588, 326
 Gallart, C., Freedman, W.L., Aparicio, A., Betelli, G., & Chiosi, C., 1999, AJ, 118, 2245
 Gallart, C., Martinez-Delgado, D., Gomez-Flechoso, M.A., & Mateo, M., 2001, AJ, 121, 2572
 Gardner, J. P. 2001, ApJ, 557, 616
 Gavazzi, G., Boselli, A., Mayer, L., Iglesias-Paramo, J., Vilchez, J.M., & Carrasco, L., 2001, ApJ, 563, L23
 Dehnen, W., & Binney, J., 1998, MNRAS, 294, 429
 Ghigna, S., Moore, B., Governato, F., Lake, G., Quinn, T., & Stadel, J., 1998, MNRAS, 300, 146
 Gill, S. P.D., Knebe, A., & Gibson, B., 2004, MNRAS, 351, 410
 Governato, F., Mayer, L., Wadsley, J., Gardner, J.P., Willman, B., Hayashi, E., Quinn, T., Stadel, J., & Lake, G., 2004, ApJ, 607, 688
 Grebel, E.K., Gallagher, J.S., & Herbeck, D., 2003, ApJ, 125, 1926
 Grebel, E.K. & Gallagher, J.S., 2004, ApJ, 610, L89
 Guhathakurta, P., Reitzel, D. B. 1998, ASP Conf. Ser. 136: Galactic Halos, 22
 Gunn, J. E., Gott, J. R. I. 1972, ApJ, 176, 1
 Haardt, F., & Madau, P., 1996, ApJ, 461, 20
 Hernandez, X., Gilmore, G., & Valls-Gabaud, D. 2000, MNRAS, 317, 831
 Hernquist L. 1993, ApJS, 86, 389
 Hogan, C.J., & Dalcanton, J.J., 2000, Phys. Rev. D., 62, 063511
 Jimenez, R., Verde, L., & Oh, S. Peng, 2003, MNRAS, 339, 243
 Kazantzidis, S., Mayer, L., Mastropietro, C., Diemand, J., Stadel, J., & Moore, B., 2004, ApJ, 608, 663
 Kleyna, J., Wilkinson, M.I., Evans, N.W., Gilmore, G., & Frayn C. 2002, MNRAS, 330, 792
 Klypin A., Zhao H., Somerville R. S. 2002, ApJ, 573, 597
 Kravtsov, A.V., Gnedin, O.Y., & Klypin, A.A. 2004, ApJ, 609, 482
 Lin, D.N.C., Jones, B.F., & Klemola, A.R. 1995, ApJ, 439, 652
 Lokas, E.L., 2002, MNRAS, 333, 697
 Lufkin, G., Quinn, T., Wadsley, J., Stadel, J., & Governato, F., 2004, MNRAS, 347, 421
 Majewski, S. R., Ostheimer, J. C., Kunkel, W. E., Johnston, K. V., Patterson, R. J., Palma, C. 1999, IAU Symp. 190: New Views of the Magellanic Clouds, 190, 508
 Maller, A.H., & Bullock, J.S., 2004, MNRAS, 355, 694
 Marcolini A., Brighenti F., D'Ercole A. 2003, MNRAS, 345, 1329, 1339
 Marcolini A., Brighenti F., D'Ercole A. 2004, submitted to MNRAS, astro-ph/0404502
 Mashchenko, S., Carignan, C., & Bouchard A., 2004, MNRAS, 352, 168
 Mastropietro, C., Moore, B., Mayer, L., Wadsley, J., & Stadel, J., 2004, submitted to MNRAS, astro-ph/0412312
 Mateo, M., 1998, ARA&A, 36, 435
 Mathewson, D. S., Ford, V. L., Schwarz, M. P., Murray, J. D.

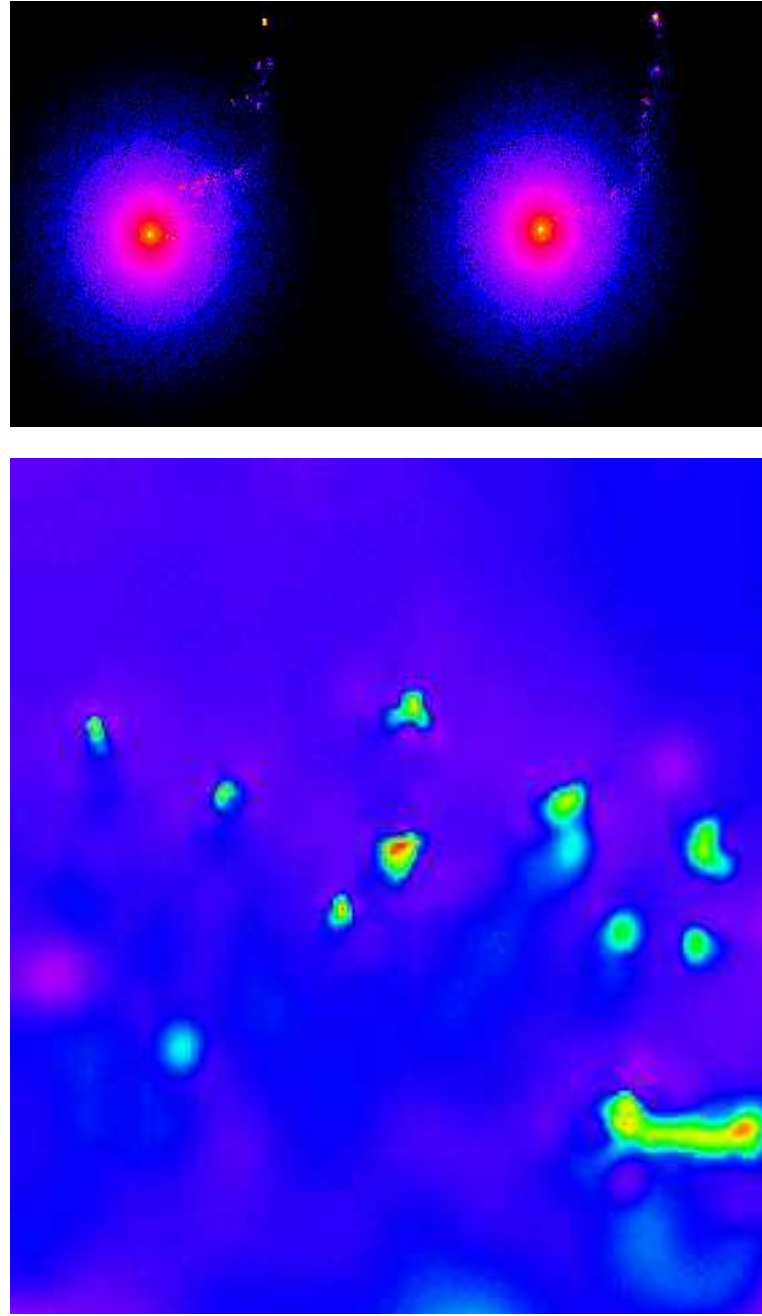


Figure 17. Top: color coded density map (brighter colors for higher densities) showing a box of 200 kpc on a side, slightly offset from the center of mass of the Milky Way+satellite system, for run Rc20RC (left) and run Rc20RCUV (right) at $t = 1.5$ Gyr. A gaseous trail fragmenting into clouds is visible. Bottom: color coded temperature map of one small region of the gaseous stream in run Rc20RC (the box has a size of about 40 kpc on a side) showing the detailed structure of the clouds.

1979, IAU Symp. 84: The Large-Scale Characteristics of the Galaxy, 84, 547

Mathewson, D. S., Wayte, S. R., Ford, V. L., Ruan, K. 1987, Proceedings of the Astronomical Society of Australia, 7, 19

Mayer, L., Governato, F., Colpi, M., Moore, B., Quinn, T., Wadsley, J., Stadel, J., Lake G. 2001a, ApJ, 547, L123

Mayer, L., Governato, F., Colpi, M., Moore, B., Quinn, T., Wadsley, J., Stadel, J., Lake G. 2001b, 559, 754

Mayer, L., Moore, B., Quinn, T., Governato, F., & Stadel, J. 2002, MNRAS, 336, 119

Mayer, L., & Wadsley, J., 2003, ASP Conference Series, Proceed-

ings of the Conference “Satellites and Tidal Streams”, La Palma 26-30 May 2003, Spain, eds, F. Prada, D. Martinez-Delgado, T. Mahoney, astro-ph/0307362

Mayer, L., 2004, Proceedings of Science, BDMH2004 (2004), 037, astro-ph/0411476

Mayer, L., & Moore, B., 2004, MNRAS, 354, 477

Mayer, L., Wadsley, J. 2004, MNRAS, 347, 277

Meurer, G. R., Bicknell, G. V., Gingold, R. A. 1985, Proceedings of the Astronomical Society of Australia, 6, 195

Moore, B., Katz, N., & Lake, G., 1996, ApJ, 457, 455

Mo, H. J., Mao, S., White, S. D. M. 1998, MNRAS, 295, 319

Mori, M., Burkert, A. 2000, ApJ, 538, 559
 Mori, M., Ferrara, A., Madau, P., 2002, ApJ, 571, 40
 Murray, S. D., White, S. D. M., Blondin, J. M., Lin, D. N. C.
 1993, ApJ, 407, 588
 Navarro J. F., Frenk C. S., White S. D. M. 1996, ApJ, 462, 563
 Navarro J. F., Frenk C. S., White S. D. M. 1997, ApJ, 490, 493
 Nulsen, P. E. J. 1982, MNRAS, 198, 1007
 Odenkirchen, M., et al. 2001, AJ, 122, 2538
 Piatek, S., et al. 2003, AJ, 126, 2346
 Quilis, V., Moore, B., Bower, R. 2000, Science, 288, 1617
 Quilis, V., Moore, B. 2001, ApJL, 555, L95
 Read, J.I & Gilmore, G., 2004, MNRAS, in press
 Shaviv, N.J., & Dekel, A., 2003, submitted to MNRAS,
 astro-ph/0305527
 Somerville, R.S., 2002, ApJ, L23
 Sommer-Larsen, J., Gotz, M., & Portinari, L., 2003, ApJ, 596, 47
 Schulz, S., Struck, C. 2001, MNRAS, 328, 185
 Sembach, K. R. 2003, preprint (astro-ph 0311089)
 Sembach, K. R. et al. 2003, ApJS, 146, 165
 Somerville, R.S., 2002, ApJ, 572, L23
 Springel V., & White S. D. M. 1999, MNRAS, 307, 162
 Springel, V., & Hernquist, L., 2003, MNRAS, 339, 289
 Susa, H., & Umemura, M., 2004 ApJ, 600, 1
 Taffoni, G., Mayer, L., Colpi, M., Governato, F. 2003, MNRAS,
 341, 434
 Thacker, R.J., & Couchman, H.M.P., 2000, ApJ, 545, 728
 Thilker, D.A., Braun, R., Walterbros, A.M., Corbelli, E., Lock-
 man, F.J., Murphy, E., & Maddalena, R., 2004, ApJ, 601,
 L39
 Thoul, A.A., & Weinberg, D.H. 1996. ApJ, 466, 608
 Tittley, E.R., Pearce, F.R., & Couchman, H.M.P., 2001, ApJ, 561,
 69
 Wadsley, J. W., Stadel, J., Quinn, T. 2004, New Astronomy, 9,
 137
 Van den Bergh, S., 1996, ApJ, 428, 617
 Verde, L., Oh, S. P., & Jimenez, R., 2002, MNRAS, 336, 541
 White, S. D. M., Frenk, C. S. 1991, ApJ, 379, 52
 Wilkinson, M., Kleyna, J.T., Evans, W.N., Gilmore, G.F., Irwin,
 M.J., & Grebel, E.K., 2004, ApJ, 611, L21